



HAL
open science

Ultraviolet emission lines in young low-mass galaxies at $z \approx 2$: physical properties and implications for studies at $z > 7$

Daniel P., Stark, Johan, Richard, Brian, Siana, Stéphane, Charlot, William R., Freeman, Julia, Gutkin, Aida, Wofford, Brant, Robertson, Rahman, Amanullah, Darach, Watson, et al.

► To cite this version:

Daniel P., Stark, Johan, Richard, Brian, Siana, Stéphane, Charlot, William R., Freeman, et al.. Ultraviolet emission lines in young low-mass galaxies at $z \approx 2$: physical properties and implications for studies at $z > 7$. Monthly Notices of the Royal Astronomical Society, 2014, 445, pp.3200 - 3220. hal-01088919

HAL Id: hal-01088919

<https://hal.science/hal-01088919>

Submitted on 29 Nov 2014

HAL is a multi-disciplinary open access archive for the deposit and dissemination of scientific research documents, whether they are published or not. The documents may come from teaching and research institutions in France or abroad, or from public or private research centers.

L'archive ouverte pluridisciplinaire **HAL**, est destinée au dépôt et à la diffusion de documents scientifiques de niveau recherche, publiés ou non, émanant des établissements d'enseignement et de recherche français ou étrangers, des laboratoires publics ou privés.

Ultraviolet emission lines in young low-mass galaxies at $z \simeq 2$: physical properties and implications for studies at $z > 7$

Daniel P. Stark,^{1★} Johan Richard,² Brian Siana,³ Stéphane Charlot,⁴
William R. Freeman,³ Julia Gutkin,⁴ Aida Wofford,⁴ Brant Robertson,¹
Rahman Amanullah,⁵ Darach Watson⁶ and Bo Milvang-Jensen⁶

¹Steward Observatory, University of Arizona, 933 N Cherry Ave, Tucson, AZ 85721, USA

²Centre de Recherche Astrophysique de Lyon, Université Lyon 1, 9 Avenue Charles Andre, F-69561 Saint-Genis Laval cedex, France

³Department of Physics and Astronomy, University of California, Riverside, CA 92521, USA

⁴UPMC-CNRS, UMR7095, Institut d'Astrophysique de Paris, 98 bis Boulevard Arago, F-75014 Paris, France

⁵Department of Physics, Stockholm University, Albanova University Centre, SE-106-91 Stockholm, Sweden

⁶Dark Cosmology Centre, Niels Bohr Institute, University of Copenhagen, Juliane Maries Vej 30, DK-2100 Copenhagen, Denmark

Accepted 2014 August 7. Received 2014 July 29; in original form 2014 May 28

ABSTRACT

We present deep spectroscopy of 17 very low mass ($M^* \simeq 2.0 \times 10^6$ – $1.4 \times 10^9 M_\odot$) and low luminosity ($M_{\text{UV}} \simeq -13.7$ to -19.9) gravitationally lensed galaxies in the redshift range $z \simeq 1.5$ – 3.0 . Deep rest-frame ultraviolet spectra reveal large equivalent width emission from numerous emission lines (N IV], O III], C IV, Si III], C III]) which are rarely seen in individual spectra of more massive star-forming galaxies. C III] is detected in 16 of 17 low-mass star-forming systems with rest-frame equivalent widths as large as 13.5 Å. Nebular C IV emission is present in the most extreme C III] emitters, requiring an ionizing source capable of producing a substantial component of photons with energies in excess of 47.9 eV. Photoionization models support a picture whereby the large equivalent widths are driven by the increased electron temperature and enhanced ionizing output arising from metal-poor gas and stars (0.04 – $0.13 Z_\odot$), young stellar populations (6–50 Myr), and large ionization parameters ($\log U = -2.16$ to -1.84). The young ages implied by the emission lines and continuum spectral energy distributions (SEDs) indicate that the extreme line emitters in our sample are in the midst of a significant upturn in their star formation activity. The low stellar masses, blue UV colours, and large specific star formation rates of our sample are similar to those of typical $z \gtrsim 6$ galaxies. Given the strong attenuation of Ly α in $z \gtrsim 6$ galaxies, we suggest that C III] is likely to provide our best probe of early star-forming galaxies with ground-based spectrographs and one off the most efficient means of confirming $z \gtrsim 10$ galaxies with the *James Webb Space Telescope*.

Key words: galaxies: evolution – galaxies: formation – galaxies: high-redshift – cosmology: observations.

1 INTRODUCTION

Low-luminosity galaxies play an important role at high redshift. Measurements of the UV luminosity function at $z \simeq 2$ indicate that more than 90 per cent of the total UV luminosity density comes from sub- L^* galaxies (e.g. Reddy & Steidel 2009; Oesch et al. 2010; Alavi et al. 2014), and the dominance of such low-luminosity systems becomes even more pronounced at yet earlier times (e.g. Bunker et al. 2010; Bouwens et al. 2012; Oesch et al. 2012; McLure et al. 2013;

Schenker et al. 2013a). The extent to which early galaxies pollute and ionize the intergalactic medium (IGM) depends sensitively on how efficiently baryons are converted to stars in the low-mass dark matter haloes thought to host the UV-faint population. But while considerable progress has been achieved in our understanding of star formation and feedback in bright L^* galaxies at $z \simeq 2$ – 3 over the past decade (see Shapley 2011 for a review), much less is known about the nature of low-luminosity systems.

Galaxy formation may well proceed very differently in this low-luminosity population. The fraction of baryons locked in stars is thought to drop rapidly for dark matter haloes less massive than $\sim 6 \times 10^{11} M_\odot$ (e.g. Conroy & Wechsler 2009;

★ E-mail: dpstark@email.arizona.edu

Guo et al. 2010; Moster et al. 2010; Behroozi, Wechsler & Conroy 2013), likely implying that the efficiency of star formation and gas cooling is greatly reduced in low-mass haloes. This deficiency is typically attributed to a combination of strong stellar feedback and photoheating from the UV background (e.g. Larson 1974; Dekel & Silk 1986; Efstathiou 1992; Murray, Quataert & Thompson 2005). When feedback is strong in low-mass haloes, star formation histories are generally found to be ‘bursty’ (e.g. Stinson et al. 2007; Hopkins et al. 2013; Shen et al. 2013; Teyssier et al. 2013). The fluctuations in star formation are predicted to occur on a dynamical time-scale and may potentially play a fundamental role in modifying the dark matter distribution in dwarf galaxies (e.g. Pontzen & Governato 2012; Teyssier et al. 2013).

If star formation is indeed very bursty in low-mass high-redshift galaxies, then we would expect their spectra to look very different from more massive L^* galaxies that have been studied in great detail (e.g. Shapley et al. 2003) at the same cosmic epoch. In the past several years, the first detailed studies targeting high-redshift galaxies with reasonably low assembled stellar masses (10^7 – $10^9 M_\odot$) have begun to emerge (e.g. Erb et al. 2010; Brammer et al. 2012; Christensen et al. 2012a,b; Maseda et al. 2013). The rest-frame ultraviolet spectra show large equivalent width (EW) nebular emission lines which are rarely seen in spectra of more massive star-forming systems (C III] $\lambda\lambda$ 1907,1909,¹ O III] $\lambda\lambda$ 1661, 1667, He II λ 1640, and C IV $\lambda\lambda$ 1548,1550), while metallicity measurements from rest-frame optical emission lines point towards metal-poor ionized gas ($\lesssim 0.2 Z_\odot$). The relative strengths of the emission lines require a much larger ionization parameter than is seen in more massive, metal-rich galaxies. It is not known what is driving the large ionization parameter or what is causing the emission lines to be so prominent. Moreover with the very small existing spectroscopic samples, it is unclear how common these ultraviolet emission features are in low-mass high-redshift galaxies.

A potentially related development is the discovery of a substantial population of $z \simeq 1.5$ – 2 low-mass star-forming galaxies with very large (200–1000 Å) rest-frame optical emission lines (e.g. Atek et al. 2011, van der Wel et al. 2011; Amorín et al. 2014; Atek et al. 2014b; Maseda et al. 2013; Masters et al. 2014). It has recently been argued that such extreme optical-line-emitting galaxies become ubiquitous among UV-selected star-forming galaxies at $z \gtrsim 4$ (e.g. Shim et al. 2011; Stark et al. 2013b; Smit et al. 2014). The EWs of [O III], H α , and H β likely require large specific star formation rates (sSFRs), as might be expected from dwarfs undergoing bursty activity. Whether these strong optical line emitters are related to the low-mass galaxies with extreme UV line emission lines described above is not yet known. If there is a connection between the two populations however, then the presence of extreme optical line emission in $z \gtrsim 6$ galaxies (Smit et al. 2014) would indicate that the UV line spectra are likely to be much richer than anticipated. Given the attenuation of Ly α in $z \gtrsim 6$ galaxies (e.g. Ono et al. 2012; Pentericci et al. 2012; Schenker et al. 2012, Schenker et al. 2014; Treu et al. 2013), the existence of prominent C III] or O III] emission might provide our best hope of characterizing low-mass $z \gtrsim 6$ galaxies with ground-based spectrographs.

¹The C III] doublet is actually a combination of [C III] λ 1907, a forbidden magnetic quadrupole transition and C III] λ 1909, a semiforbidden electrodipole transition. In low-resolution optical spectra of $z \simeq 2$ galaxies, the doublet is not resolved. For the remainder of this paper, we will refer to the line as either the blended C III] λ 1908 doublet or simply as C III].

Clearly a much larger spectroscopic data base of low-mass galaxies is required to clarify the implications of the observations described above. Fortunately with the large samples of faint gravitationally lensed galaxies that are now being discovered with deep imaging and grism spectroscopy from the *Hubble Space Telescope* (HST; e.g. Limousin et al. 2007; Richard et al. 2007; Bradley et al. 2013; Atek et al. 2014a; Coe, Bradley & Zitrin 2014; Schmidt et al. 2014), it is becoming feasible to explore the properties of sizeable samples of low-mass galaxies with unprecedented detail. In Alavi et al. (2014), a sample of ultrafaint gravitationally lensed galaxies in the Abell 1689 field was presented, demonstrating that the luminosity function rises steeply towards $M_{UV} = -13$ at $z \simeq 2$. Here, we build on this progress by using Keck, Very Large Telescope (VLT), and Magellan to obtain deep optical and near-infrared spectra for a subset of the faint lensed galaxies in Abell 1689 and similarly faint samples in two other cluster fields (MACSJ0451+0006 and Abell 68).

These spectra will allow us to determine whether the prominent UV emission lines seen in Erb et al. (2010) and Christensen et al. (2012a,b) are common in low-mass star-forming galaxies at high redshift. Through characterization of the rest-optical emission lines, we will examine whether galaxies with large EW UV emission lines have similar optical emission-line spectra to the extreme line emitters reported in Atek et al. (2011) and van der Wel et al. (2011). Using photoionization models, we will attempt to understand what the powerful UV emission lines tell us about the nature of low-mass galaxies at high redshift. Our ultimate goals are twofold. First, we seek to understand whether the spectra of low-mass galaxies are consistent with the picture of bursty star formation expected with strong stellar feedback. And secondly, motivated by the very low success rate in recovering Ly α at $z \gtrsim 6$, we aim to determine whether UV lines such as C III], C IV, and O III] might be detectable in $z \gtrsim 6$ galaxy spectra.

The paper is organized as follows. In Section 2, we describe the optical spectroscopic observations undertaken with Keck and the VLT and then discuss the sample selection, multiwavelength imaging, magnification, and distribution of UV luminosities. In Section 3, we discuss the EW distribution and flux ratios of UV emission lines of our sample of lensed galaxies. With the goal of understanding what drives the UV emission-line strengths, we characterize the stellar masses, UV continuum slopes, metallicities, and relative chemical abundances of our sample in Section 4. In Section 5, we use photoionization models to investigate what range of properties (metallicity, age, ionization parameter) are required to reproduce the UV emission-line spectra of our low-mass sample. Finally, in Section 6, we assess implications for star formation in low-mass galaxies at $z \simeq 2$ – 3 and discuss the feasibility and physical motivation for detecting lines other than Ly α with existing samples of $z \gtrsim 6$ galaxies. We summarize our conclusions in Section 7.

Throughout the paper, we adopt a Λ -dominated, flat universe with $\Omega_\Lambda = 0.7$, $\Omega_M = 0.3$, and $H_0 = 70 h_{70} \text{ km s}^{-1} \text{ Mpc}^{-1}$. We use a solar oxygen abundance of $12 + \log(O/H) = 8.69$ (Asplund et al. 2009). All magnitudes are quoted in the AB system (Oke et al. 1983).

2 OPTICAL SPECTROSCOPY AND MULTIWAVELENGTH IMAGING

In this section, we introduce an ongoing spectroscopic programme targeting low-luminosity gravitationally lensed galaxies at high redshift. We describe Keck observations in Section 2.1 and VLT observations in Section 2.2. In Section 2.3, we present the final

Table 1. Details of optical spectroscopic observations. From left to right: cluster field, instrument used, instrument setup, observation dates, and total exposure time. For the Keck/LRIS observations, the blue side setup is denoted as ‘B’ and red side as ‘R’.

Cluster	Instrument	Setup	Dates	t_{exp} (ks)
MACS 0451	FORS2	G300V	27 Jan 2012	8.1
MACS 0451	FORS2	G300V	28 Jan 2012	10.8
Abell 68	FORS2	G300V	20 Oct 2011	5.40
Abell 68	FORS2	G300V	15 Nov 2011	2.70
Abell 68	FORS2	G300V	18 Jul 2012	2.70
Abell 68	FORS2	G300V	19 Jul 2012	8.10
Abell 1689	FORS2	G300V	19 Feb 2012	2.70
Abell 1689	FORS2	G300V	20 Feb 2012	2.70
Abell 1689	FORS2	G300V	21 Feb 2012	2.70
Abell 1689	FORS2	G300V	15 Mar 2012	2.70
Abell 1689	FORS2	G300V	17 Mar 2012	2.70
Abell 1689	FORS2	G300V	18 Mar 2012	2.70
Abell 1689	FORS2	G300V	25 Mar 2012	2.70
Abell 1689	LRIS	400/3400 (B)	9 May 2010	18.0
–	–	600/7500 (R)	–	12.6
Abell 1689	LRIS	400/3400 (B)	24 Feb 2012	9.0
–	–	600/7500 (R)	–	5.9

spectroscopic sample. We describe multiwavelength imaging data sets in Section 2.4, discuss the lensing magnifications and source luminosities in Section 2.5, and present Magellan near-IR spectroscopy of a subset of our sample in Section 2.6.

2.1 Keck/LRIS

Optical spectra of lensed galaxies in the Abell 1689 field were obtained with the Low Resolution Imaging Spectrometer (LRIS; Oke et al. 1995) on the Keck I telescope on 2010 May 09 and 2012 February 24. Both nights were clear and the seeing was 0.7 (May 2010) and 1.0 arcsec (Feb 2012). The slit width was 1.2 arcsec for both masks. A dichroic was used to split the light at 5600 Å between the two arms of the spectrograph. On the blue side, a grism with 400 lines mm⁻¹ blazed at 3400 Å was used, and on the red side, the 600 lines mm⁻¹ grating blazed at 7500 Å was used. For the 1.2 arcsec slit width used for both masks, this results in a blue side resolution of 8.2 Å and a red side resolution of 5.6 Å. To reduce read noise, the blue side CCD was binned by a factor of 2 in the spatial direction. The blue and red side exposures were 1800 and 740 s, respectively. Total integration times were 18 (blue) and 12.6 ks (red) for the 2010 May observations and 9.0 (blue) and 5.9 ks (red) for the 2012 February observations. The individual exposures were rectified, cleaned of cosmic rays, and stacked using the pipeline of Kelson (2003). The one-dimensional spectra were optimally extracted using the Horne (1986) algorithm. Details are summarized in Table 1.

2.2 VLT/FORS2

The FORS2 spectrograph on the VLT UT1 (Antu) was used to target lensed background galaxies in the field of three massive clusters: MACSJ0451+0006 (hereafter MACS 0451), Abell 68, and Abell 1689. The observations were performed as part of ESO programme 088.A-0571 (PI: Richard), where we set up FORS2 in MXU mode to allow for more flexibility when targeting the most magnified sources near the cluster centre. We used the combination of the G300V grism and the order filter GG435 to cover the wavelength range

3800–9500 Å with a spectral resolution of 10.3 Å as measured from the full width at half-maximum of bright isolated sky lines. Seeing ranged between 0.8 and 0.9 arcsec for all three masks. A summary of basic observational details is provided in Table 1. The FORS reduction pipeline was used to perform flat-fielding, wavelength calibration, sky subtraction, and object extraction. Flux calibration was performed using standard A0V stars.

2.3 Lensed galaxy sample

The Keck and VLT slit masks were filled with gravitationally lensed galaxies spanning a range of redshifts and magnitudes. We have targeted galaxies with and without spectroscopic redshifts. Systems with known redshifts were identified through earlier campaigns targeting multiply-imaged systems (e.g. Santos et al. 2004; Broadhurst et al. 2005; Frye et al. 2007; Richard et al. 2007). Redshift confirmation of the input spectroscopic sample was achieved through identification of Ly α emission or interstellar UV absorption lines. The remaining slits were devoted to multiply-imaged galaxies without confirmed redshifts.

We isolate a subset of these for analysis in this paper using three basic selection criteria. First, to ensure that emission-line measurements are made at the correct rest-frame wavelengths, we only consider galaxies with robust spectroscopic redshifts. Most galaxies that fall in our ‘robust’ category have their redshift confirmed from two separate spectral features (i.e. Ly α emission and metal absorption or continuum break). For several systems, the spatial extent and asymmetry of Ly α prove sufficient for redshift confirmation. Any galaxies on the Keck and VLT masks lacking a confident redshift determination are excised from the sample.

Secondly, we require that C III] falls in the spectral window covered by the Keck and VLT spectra. This criterion restricts the redshift range to $1.3 < z < 4.0$. Objects outside this redshift range are not included in our sample. We also excise objects with redshifts which place the primary emission lines of interest under strong atmospheric OH lines. As the sky lines are strongest in the red side of the optical, this primarily impacts galaxies at $z \gtrsim 2.5$.

And finally, to ensure reliable emission-line EW measurements, we only consider galaxies with UV continuum detections in the spectra. Given the depth of the spectra, this requirement has the effect of limiting our sample to galaxies with apparent optical magnitudes brighter than $m \simeq 25$ –26, placing a lower threshold on the UV flux of galaxies in our sample. While there are several fainter objects on our masks with confirmed redshifts (from Ly α), the faint continuum dictates that additional emission lines can only be detected if EWs are very large (i.e. > 50 Å rest frame), well in excess of the EWs expected for the UV metal lines. Examination of the spectra of the faint Ly α emitters that we excise from our sample confirms the absence of additional emission lines at the 50 Å level.

After removing galaxies that do not satisfy the three criteria listed above, we are left with a sample of 17 lensed galaxies. As we will discuss in Section 3, the rest-ultraviolet spectra of 16 of the 17 galaxies reveal C III] emission. Colour images of the 16 C III] emitters are shown in Fig. 1. The redshifts range between $z = 1.599$ and 2.976. The spectral features used for redshift identification are listed in Table 2. The sample is comprised of 4 galaxies from the MACS 0451 field, 2 galaxies from the Abell 68 field, and 11 galaxies from Abell 1689 field. While the MACS 0451 and Abell 68 observations are entirely based on VLT spectra, the spectroscopic sample towards Abell 1689 is made up of a mixture of Keck and VLT spectra. Nine galaxies have deep Keck spectra, and five have

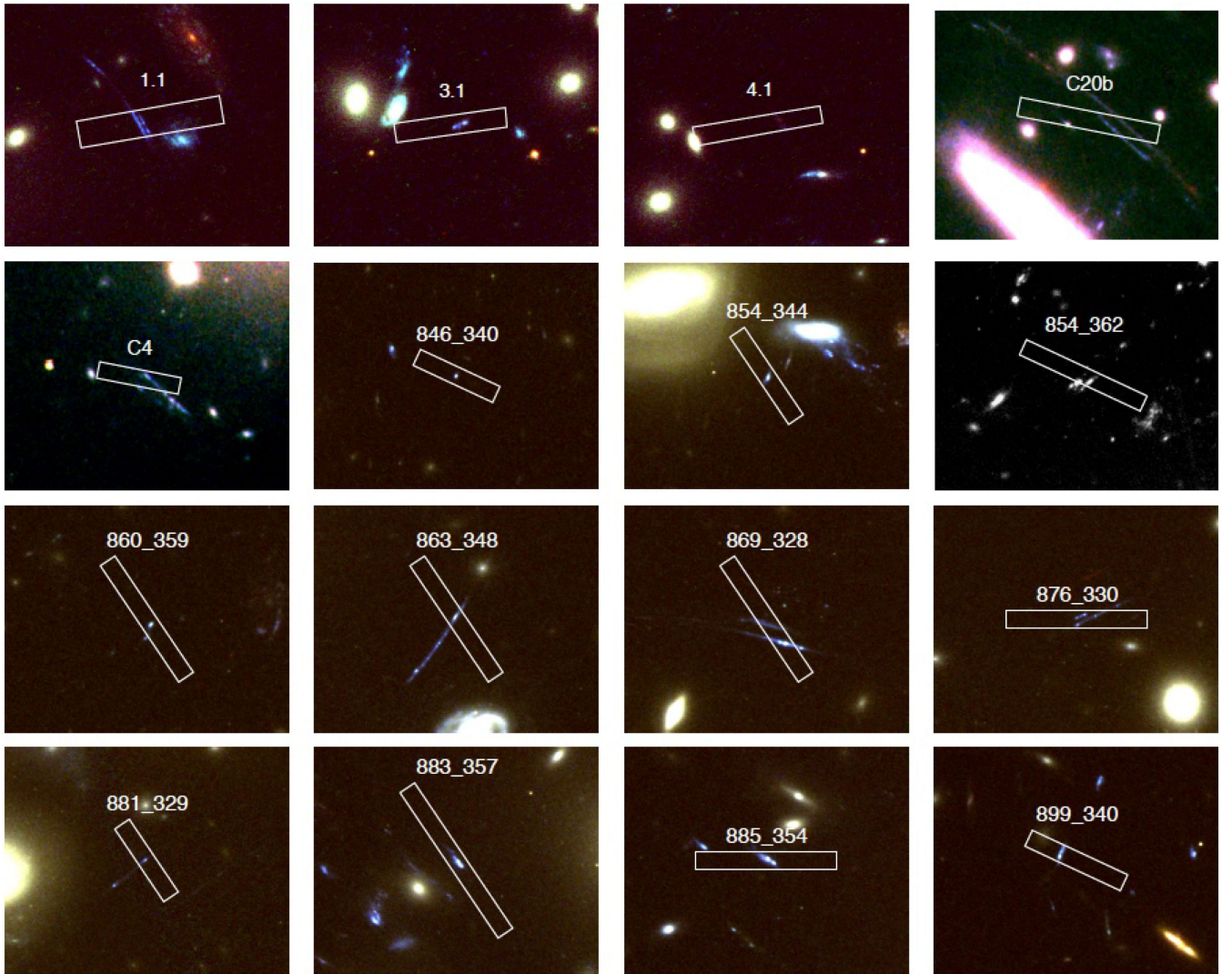


Figure 1. Colour images of the 16 dwarf star-forming galaxies at $1.6 \lesssim z \lesssim 3.0$. All of the galaxies have strong collisionally excited emission lines in the rest-frame ultraviolet. We overlay the PA and slit positions of the Keck/LRIS and VLT/FORS spectra.

deep VLT spectra. For the three systems with both Keck and VLT observations, we examine both spectra, ensuring that the redshift identifications and emission-line measurements are consistent.

2.4 Multiwavelength imaging

Abell 1689 is the most well-studied cluster field in our sample. The optical portion of the SED is well sampled by deep *HST*/Advanced Camera for Surveys (ACS) imaging in four filters (*F475W*, *F625W*, *F775W*, *F850LP*). Details of the Abell 1689 ACS data set have been provided in Broadhurst et al. (2005). The near-infrared is constrained by a combination of *HST*/WFC3 imaging (*F105W*, *F125W*, *F140W*, *F160W*) and K_s -band imaging from the Infrared Spectrometer and Array Camera formerly installed at the VLT. For several sources, we also use constraints from HAWK-I photometry in the K band from VLT programme 181.A-0185 (PI: Cuby). Deep *Spitzer*/IRAC data (total exposure time of 5 h) have been obtained on Abell 1689 through the *Spitzer* programme 20439 (PI: Egami). We have used the publicly available Basic Calibrated Data from the *Spitzer* archive.

While not as well studied as Abell 1689, the cluster MACS 0451 has been imaged in four filters by *HST*. Deep ACS optical imaging has been taken in the *F606W* and *F814W* filters through programmes 10491 and 12166 (PI: Ebeling). In the near-infrared, deep WFC3/IR imaging has been acquired in the *F110W* and *F140W* filters through programme number 10875 (PI: Ebeling). *Spitzer*/IRAC imaging in the [3.6] and [4.5] bandpasses has been taken through IRAC cluster lensing programme (ID 60034, PI: Egami).

Abell 68 has been observed with multiple optical and near-infrared filters with *HST*. Deep R -band (*F702W*) imaging was obtained with the Wide Field Planetary Camera during *HST* Cycle 8 (programme 8249, PI: Kneib). Details of the reduction of the *F702W* imaging are provided in Smith et al. (2005). Additionally, Abell 68 has been imaged with ACS in the *F814W* filter, and in the near-infrared *F110W* and *F160W* filters with WFC3/IR as part of *HST* programme 11591 (PI: Kneib).

All *HST* data have been combined using the MULTIDRIZZLE software (Koekemoer et al. 2007) and aligned to the same astrometric reference frame. For the *Spitzer* data, we have used the publicly available Basic Calibrated Data mosaicked on to a 0.6 arcsec pixel scale.

Table 2. Properties of spectroscopic sample of lensed galaxies presented in this paper. Each galaxy has a deep Keck/LRIS (Section 2.1) or VLT/FORS2 (Section 2.2) spectrum. We report V_{606} -band magnitudes in MACS 0451 and R_{702} -band magnitudes in Abell 68. In Abell 1689, we report i_{775} -band magnitudes for all sources where available. The lensing flux magnification (μ) are derived from up-to-date cluster mass models (see Section 2.5 for references). The rest-UV spectrum of 876_330 was presented in Christensen et al. (2012a), where it was denoted Abell 1689 arc 31.1. The primary means of redshift identification is listed in the rightmost column. ‘IS abs’ refers to UV metal absorption lines, ‘break’ denotes detection of a Ly α continuum break, ‘Metal em’ refers to UV emission from metallic species (i.e. O III] λ 1661,1667, C III] λ 1908), and ‘Opt em’ denotes rest-optical emission lines (i.e. H α , [O III] λ 5007). Five of the galaxies listed above are multiple images. These include 881_329 (image 36.1 in Limousin et al. 2007), 885_354 (image 22.3), 863_348 (image 12.2), 876_330 (image 31.1), 854_344 (image 17.3).

Name	z_{spec}	RA	Dec.	m_{AB}	μ	M_{UV}	$W_{\text{Ly}\alpha,0}$ (\AA)	$W_{\text{C III],0}$ (\AA)	Redshift-ID
MACS 0451									
1.1	2.060	04:51:53.399	+00:06:40.31	22.1	45.0 ± 2.5	-18.6 ± 0.1	–	6.7 ± 0.6	IS abs, Opt em
6.2	1.405	04:51:53.592	+00:06:24.96	21.7	14.7 ± 1.8	-19.4 ± 0.1	–	<1.2	IS abs, Opt em
4.1	1.810	04:51:54.488	+00:06:49.01	25.6	5.8 ± 1.2	-17.1 ± 0.2	–	10.0 ± 2.4	IS abs, Metal em
3.1	1.904	04:51:55.438	+00:06:41.16	23.7	25.2 ± 4.9	-17.5 ± 0.2	–	2.0 ± 0.7	Opt em
Abell 68									
C4	2.622	00:37:07.657	+09:09:05.90	24.8	46 ± 7	-16.3 ± 0.2	36.6 ± 5.7	6.7 ± 2.1	Ly α em, Metal em
C20b	2.689	00:37:05.405	+09:09:59.14	23.3	90 ± 12	-17.1 ± 0.2	>19.9	>10.4	Ly α em, Metal em
Abell 1689									
881_329	1.559	13:11:31.543	–01:19:45.88	25.9	75.1 ± 12.4	-13.7 ± 0.2	–	7.1 ± 3.1	Metal em
899_340	1.599	13:11:35.705	–01:20:25.22	23.9	7.5 ± 1.3	-18.2 ± 0.2	–	5.1 ± 1.4	Metal em, Opt. em
883_357	1.702	13:11:31.882	–01:21:26.10	23.3	13.0 ± 1.4	-18.4 ± 0.1	76.0 ± 18.8	6.5 ± 0.7	Ly α em, Metal em
860_359	1.702	13:11:26.426	–01:21:31.22	24.5	4.3 ± 0.3	-18.4 ± 0.1	163.8 ± 25.5	12.4 ± 1.5	Ly α em, Metal em
885_354	1.705	13:11:32.405	–01:21:15.98	23.2	15.5 ± 3.0	-18.3 ± 0.2	35.7 ± 4.6	3.9 ± 0.6	Ly α em, IS abs
863_348	1.834	13:11:27.350	–01:20:54.82	24.1	35 ± 3.7	-16.6 ± 0.1	73.1 ± 8.6	13.5 ± 1.6	Ly α em, Metal em
876_330	1.834	13:11:30.320	–01:19:51.13	24.1	27 ± 3.1	-16.9 ± 0.2	>50.0	10.0 ± 2.7	Ly α em, Metal em
869_328	2.543	13:11:28.690	–01:19:42.69	23.3	270 ± 61	-15.8 ± 0.3	4.3 ± 0.4	1.8 ± 0.3	Ly α em, IS abs
854_344	2.663	13:11:24.982	–01:20:41.57	23.4	6.2 ± 0.3	-19.9 ± 0.1	45.3 ± 2.7	>4.0	Ly α em, IS abs
854_362	2.731	13:11:24.982	–01:21:43.53	24.3	2.8 ± 0.1	-19.9 ± 0.1	129.6 ± 21.8	12.0 ± 3.2	Ly α em, C III] em
846_340	2.976	13:11:23.141	–01:20:23.08	25.3	2.5 ± 0.1	-19.2 ± 0.1	86.4 ± 24.8	>10.3	Ly α em, break

2.5 Magnification and UV luminosity

Lensing magnifications (μ) for each source are presented in Table 2. The magnification factors and associated uncertainties are computed up-to-date cluster mass models using the LENSTOOL program (Kneib 1993; Jullo et al. 2007). The cluster mass model used for Abell 1689 is based on Limousin et al. (2007) but is updated to include new spectroscopic redshifts of multiply-imaged galaxies. The mass model in Abell 68 is described in Richard et al. (2007, 2010), while the MACS 0451 mass model is based on that presented in Jones et al. (2010), updated to include the new multiple images presented in this work. Magnification factors range between $\mu = 2.5$ and 270. The median magnification is $\mu = 15.5$.

The apparent optical magnitudes (V_{606} in MACS 0451, R_{702} in Abell 68, and i_{775} in Abell 1689) span $m_{\text{AB}} = 21.7$ and 25.9 (see Table 2) with an average of $m_{\text{AB}} = 23.9$. Without the magnification provided by lensing, this sample would have had an average apparent magnitude of $m_{\text{AB}} = 26.9$, which is much too faint for spectroscopic detection of low-EW emission features. The absolute UV magnitudes of our sample range between $M_{\text{UV}} = -13.7$ and -19.9 with a median of $M_{\text{UV}} = -18.2$. In addition to being considerably less luminous than most spectroscopic samples of unlensed UV-selected galaxies at $z \simeq 2-3$ (which generally span $M_{\text{UV}} \simeq -20.0$ to -22.5), the galaxies in our sample are also intrinsically fainter than the large population of lensed systems that have been uncovered in the Sloan Digital Sky Survey (e.g. Belokurov et al. 2009; Diehl et al. 2009; Bayliss 2012; Stark et al. 2013a). Deep spectra of the low-luminosity galaxies in our sample thus provide a very complementary picture to existing samples of luminous lensed galaxies with deep rest-UV spectra

(e.g. Pettini et al. 2002; Quider et al. 2009, 2010; Bayliss et al. 2014; James et al. 2014).

2.6 Near-infrared spectroscopy

We have obtained near-infrared spectra of four of the galaxies in Table 2 using the Folded-port InfraRed Echellette (FIRE; Simcoe et al. 2013) on the 6.5 m Magellan Baade Telescope. An additional galaxy in our sample (860_359) was observed for 1 h with the XSHOOTER spectrograph (Vernet et al. 2011) on the VLT as part of ESO programme 085.A-0909 (PI: Watson). Details on the observational setup can be found in Amanullah et al. (2011).

A summary of the FIRE observations is presented in Table 3. Magellan/FIRE data were collected on UT 2012 February 16, October 29, and 2013 May 01. The typical seeing during the observations conducted on 2012 February 15 and October 28 was 0.5 and 0.8 arcsec, respectively. Conditions were variable on 2013 May 01 with seeing varying between 0.6 and 1.3 arcsec. We used the echelle

Table 3. Summary of Magellan/FIRE near-infrared spectroscopic observations of lensed galaxies listed in Table 2. PA of the slit is given in degrees E of N.

Cluster	Target	Date	t_{exp} (ks)	PA (deg)
MACS 0451	1.1a	16 Feb 2012	2.7	125
MACS 0451	1.1b	29 Oct 2012	3.0	30
MACS 0451	6.2	16 Feb 2012	1.2	120
MACS 0451	3.1	16 Feb 2012	0.6	120
Abell 1689	899_340	01 May 2013	3.6	345

mode throughout both nights, providing spectral coverage between 0.8 and 2.4 μm . We used a 0.75 arcsec slit on 2012 February 16 and 2013 May 01, delivering a resolving power of $R = 4800$. Skylines in the 2012 February data are measured to have a Gaussian σ of 0.9 and 1.9 \AA at 1.1 and 2.2 μm , respectively. In the 2013 May data, we measure $\sigma \simeq 1.3$ and 2.2 \AA at 1.1 and 2.2 μm . The spectra collected on 2012 October 28 were obtained with a 1.0 arcsec slit width, providing a somewhat coarser spectral resolution ranging between $\sigma \simeq 1.5$ and 2.5 \AA between 1.1 and 2.2 μm .

Reduction of the Magellan/FIRE spectra was performed using the FIREHOSE IDL pipeline developed for FIRE. Wavelength calibration was achieved using Th+Ar reference arc lamps. For telluric absorption and relative flux calibration, we used spectral observations of A0V standard stars. One-dimensional flux and error spectra are extracted interactively for each object using an aperture defined by the positions and widths of the rest-optical emission lines present in individual exposures.

3 REST-FRAME ULTRAVIOLET SPECTRA

We show a subset of our highest quality optical spectra in Fig. 2. The most notable features of the spectra shown in Fig. 1 are the ubiquitous presence of ultraviolet emission lines (i.e. C IV, O III], C III]) and the near-absence of low- and high-ionization interstellar absorption lines (i.e. Si II, C II, Si IV, C IV, Al II) which commonly appear in ultraviolet spectra. In this paper, most of our discussion will focus on the emission lines. A detailed analysis of the absorption-line properties will appear in a subsequent paper.

3.1 Characterization of emission lines

In each of the 17 galaxies in our sample, we search for emission from Ly α λ 1216, N V λ 1240, N IV] λ 1487, C IV $\lambda\lambda$ 1548,1550, He II λ 1640, O III] $\lambda\lambda$ 1661,1667, N III] λ 1750, Si III] $\lambda\lambda$ 1883,1892,

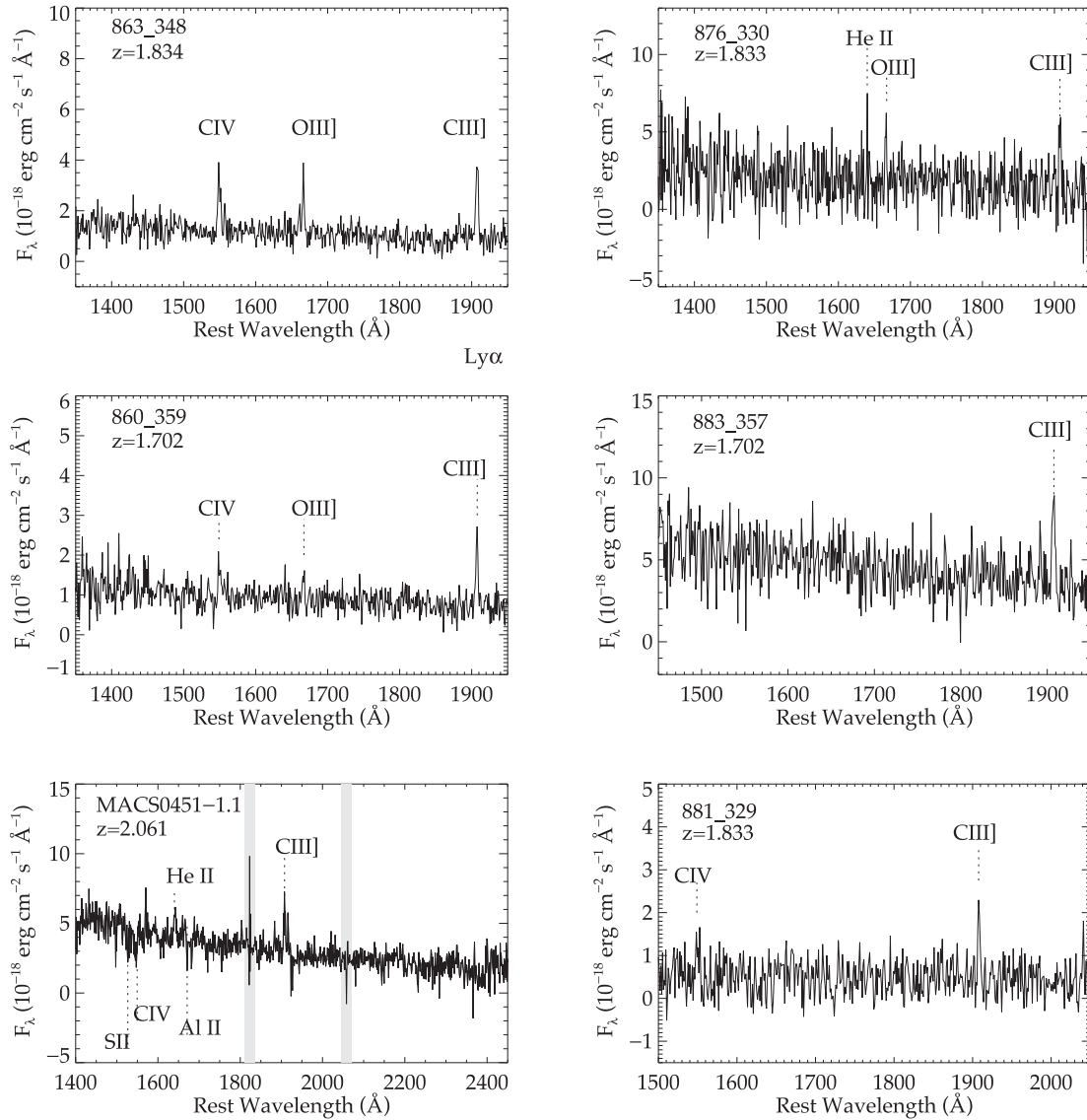


Figure 2. Prominent emission lines in rest-UV spectra of intrinsically faint gravitationally lensed galaxies. The strongest line is typically the blended C III] λ 1908 doublet, but we often note emission from the blended C IV λ 1549 doublet, He II λ 1640, O III] $\lambda\lambda$ 1661,1666, and Si III] $\lambda\lambda$ 1883,1892. The fluxes are as observed, with no adjustment for lensing magnification. Vertical grey swaths in MACS 0451-1.1 correspond to wavelengths with strong sky residuals.

and the blended C III] λ 1908 doublet. While no significant N V or N III] emission is detected in any of our galaxies, each of the other lines is present in at least one of the galaxies in our sample.

If an emission feature is detected significantly, line fluxes are determined through Gaussian fits to the observed emission. For each emission-line detection, the 1σ error in the line flux is determined through bootstrap resampling of the line within the allowed uncertainties. In most cases, the continuum is detected with significance, allowing EWs to be reliably determined. In the few cases in which the continuum is detected at low significance ($S/N < 2$), we measure the 2σ continuum flux density limit near the wavelength of the emission line in question, allowing us to place a lower limit on the emission-line EW. Finally, in cases where the continuum is significantly detected but no flux from the emission line is detected, we note 2σ upper limits on the flux and EW. The median 3σ flux limit for C III] is 4.3×10^{-18} erg cm $^{-2}$ s $^{-1}$. In the highest quality spectra, the line flux limit is as low as 1.8×10^{-18} erg cm $^{-2}$ s $^{-1}$. We measure C III] fluxes ranging between 2.2×10^{-18} and 2.0×10^{-17} erg cm $^{-2}$ s $^{-1}$.

3.2 C III] EW distribution

We find that the strongest rest-UV emission line (other than Ly α) is always the blended C III] λ 1908 doublet. In 16 of our 17 galaxies, the C III] emission line is significantly detected. The mean C III] EW of our sample (see Table 2 for individual values) is 7.1 Å, similar to the value reported for the metal-poor $z = 2.3$ star-forming galaxy in Erb et al. (2010). We note that unlike the SFR or stellar mass, the EW requires no adjustment for magnification. In Fig. 3, we present the distribution of C III] EWs (including results from BX 418 from Erb et al. 2010 and M2031 from Christensen et al. 2012a). The composite UV spectrum of 811 $z \simeq 3$ LBGs in Shapley et al. (2003) provides a useful comparison. This population is on average intrinsically brighter than the star-forming dwarf galaxies considered in this paper. While the Shapley et al. (2003) composite

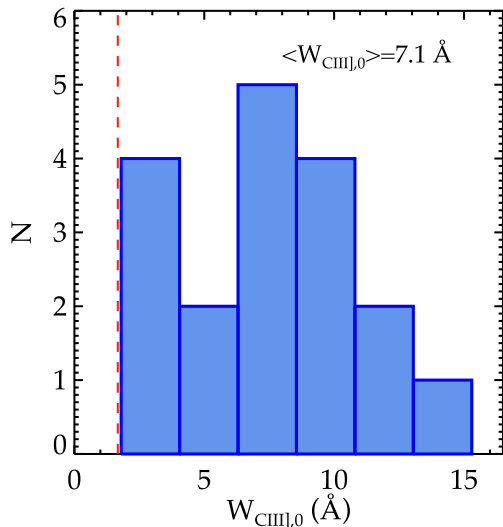


Figure 3. Rest-frame C III] λ 1908 EW distribution in low-luminosity gravitationally lensed galaxies at $z \simeq 1.5$ – 3.0 . We include the 16 C III] emitters in our sample and two similar systems (BX418 and M2031) reported in Erb et al. (2010) and Christensen et al. (2012a). The galaxies included here are metal poor with large sSFRs and blue UV slopes. The red dashed line shows the C III] EW measured in the Shapley et al. (2003) composite spectrum of $z \simeq 3$ LBGs.

LBG spectrum yields a significant detection of C III] λ 1908, the EW (1.67 Å) is more than a factor of 4 lower than the average of the low-luminosity star-forming galaxies in Table 2.

But while low-luminosity galaxies are certainly offset towards larger C III] EWs with respect to more luminous systems, it is clear from Fig. 3 that there is a considerable dispersion in the EW distribution. On one hand, our sample includes a population of ‘extreme’ C III] emitters with EWs ranging between 10.0 and 13.5 Å. But there are also low-luminosity star-forming systems in our sample with C III] EWs of just 1.8–3.9 Å. In the following sections, we will attempt to understand both why C III] EWs appear to be larger in low-luminosity star-forming systems and what physically is driving the large scatter in the C III] EW distribution.

3.3 Additional rest-UV emission lines in C III] emitters

While C III] is typically the strongest emission line other than Ly α in the rest-UV spectra of low-luminosity galaxies at high redshift, the spectra shown in Fig. 2 reveal additional emission features. By characterizing the flux ratios of the ultraviolet emission lines, we can gain additional insight into the ionized gas physical conditions and stellar populations of our sample of dwarf star-forming galaxies. In Table 4, we list the flux ratios relative to C III] for galaxies in our sample with high-quality spectra.

Perhaps the most striking feature in the rest-UV spectra shown in Fig. 2 is the presence of C IV $\lambda\lambda$ 1548,1550 emission, indicating that the ionizing spectra of several dwarf star-forming galaxies in our sample have a substantial flux of photons with energies in excess of 47.9 eV, similar to what is often inferred from spectroscopy of nearby blue compact dwarf galaxies (e.g. Guseva, Izotov & Thuan 2000; Thuan & Izotov 2005; Shirazi & Brinchmann 2012). Accurate identification of C IV emission in high-redshift star-forming galaxies is often compromised in low-resolution spectra by overlapping interstellar and P-Cygni absorption, but the absence of strong absorption features in many of our galaxies gives us a rare unobscured measure of the C IV strength. The C IV/C III] flux ratio is largest (0.8 ± 0.1) in the $z = 1.863$ galaxy 863_348, the most extreme C III] emitter in our sample. Two other C III] emitters in our sample show C IV detections with C IV/C III] flux ratios of 0.4 (860_359) and 0.5 (881_329). The rest-frame C IV EWs of these three systems span 3.3–8.1 Å.

Ultimately we would like to characterize the distribution of nebular C IV/C III] flux ratios (an indicator of the hardness of the ionizing spectrum) in dwarf star-forming galaxies. While C IV is only

Table 4. Rest-UV emission flux ratios (relative to the blended C III] λ 1908 doublet). If line is not detected significantly, we list the 2σ upper flux ratio limit. No C IV λ 1549 flux measurement is possible for MACS0451-1.1 owing to prominent interstellar absorption feature.

	A1689	A1689	A1689	M0451	A1689
$f_{\text{line}}/f_{\text{C III]}}$	876_330	863_348	860_359	1.1	881_329
N V λ 1240	$\lesssim 1.1$	$\lesssim 0.2$	$\lesssim 0.6$	–	$\lesssim 2.9$
N IV] λ 1487	0.5 ± 0.2	$\lesssim 0.1$	$\lesssim 0.1$	–	$\lesssim 0.7$
C IV λ 1549	$\lesssim 0.6$	0.8 ± 0.1	0.4 ± 0.1	–	0.5 ± 0.3
He II λ 1640	$\lesssim 0.5$	$\lesssim 0.1$	$\lesssim 0.2$	0.5 ± 0.1	$\lesssim 0.5$
O III] λ 1661	$\lesssim 0.4$	0.2 ± 0.1	$\lesssim 0.2$	0.2 ± 0.1	$\lesssim 0.5$
O III] λ 1666	0.5 ± 0.2	0.6 ± 0.1	0.3 ± 0.1	0.3 ± 0.1	$\lesssim 0.5$
N III] λ 1750	$\lesssim 0.3$	$\lesssim 0.1$	$\lesssim 0.1$	$\lesssim 0.1$	$\lesssim 0.3$
[Si III] λ 1883	$\lesssim 0.3$	0.2 ± 0.1	0.1 ± 0.1	0.2 ± 0.1	$\lesssim 0.5$
[Si III] λ 1892	$\lesssim 0.3$	$\lesssim 0.1$	0.1 ± 0.1	0.2 ± 0.1	$\lesssim 0.5$

significantly detected in 3 of 17 systems, it should be emphasized that non-detection of C IV in our sample does not necessarily indicate a low ($\lesssim 0.5$) C IV/C III] ratio. Given that C IV appears to typically be at least a factor of 2 fainter than C III], we can only detect C IV emission in those galaxies with very large EW C III] emission. In the eight galaxies with rest-frame C III] EWs in excess of 7.0 Å, three systems have C IV detections with C IV/C III] flux ratios greater than 0.4 (881_329, 860_359, 863_348). One of the undetected galaxies has a strong C IV absorption component (854_362) which precludes identification of nebular emission in our low-resolution spectra. In the remaining four, we place 2σ upper limits of 0.6–2.3 on the C IV/C III] flux ratios and thus cannot rule out the presence of C IV at 40–50 per cent the flux of C III]. Thus, among the large EW C III] emitters, powerful C IV emission appears to be present with a C IV/C III] flux ratio greater than 0.4 at least 50 per cent of the time.

Given that the energy required to doubly ionize helium (54.4 eV) is only slightly greater than the energy required to triply ionize carbon (47.9 eV), we might expect to detect nebular He II $\lambda 1640$ emission in several of the extreme C IV-emitting galaxies in our sample. But as is clear from Fig. 2, many of the extreme C III]- and C IV-emitting galaxies in our sample do not have detectable He II emission. The best limit comes from the lack of strong He II emission in 863_348, the galaxy with the largest EW C III] and C IV emission. Adopting a 2σ upper limit on the He II flux, we find that 863_348 has an He II/C III] ratio of $\lesssim 0.1$ and a rest-frame EW of $\lesssim 1.4$ Å. The only confident He II detection is in the C III]-emitting galaxy MACS 0451-1.1. The He II/C III] flux ratio in this system (0.5 ± 0.1) is very similar to that found for the metal-poor galaxy BX 418 in Erb et al. (2010). As with BX 418, stellar winds might contribute significantly to the He II line in MACS 0451-1.1. A higher resolution (and larger S/N) spectra would be required to disentangle the nebular and stellar components of the line.

After C III], the most commonly detected emission line (other than Ly α) is the O III] $\lambda\lambda 1661, 1666$ doublet. We commonly detect O III] $\lambda 1666$ emission with fluxes as large as 50–60 per cent those of C III]. The O III] $\lambda 1661$ emission line is generally weaker than O III] $\lambda 1666$, with fluxes typically not greater than 20 per cent those of C III]. Among the five systems with the best quality spectra (and those listed in Table 4), rest-frame EWs range between $\lesssim 0.5$ and 1.5 Å for O III] $\lambda 1661$ and 1.2 and 7.4 Å for O III] $\lambda 1666$. The O III] $\lambda 1666$ EWs in our sample are considerably greater than the EW (0.23 Å) measured in luminous star-forming galaxies at $z \simeq 3$ (Shapley et al. 2003). The most extreme UV line emitters (863_348, 876_330), show O III] $\lambda 1666$ emission with EWs between three and six times greater than that measured in the metal-poor star-forming system BX 418 (Erb et al. 2010).

We also note the presence of weak emission from N IV] $\lambda 1487$ and Si III] $\lambda\lambda 1883, 1892$ in several of our sources. Where detected, the Si III] doublet typically is seen with a flux of 10–20 per cent that of C III]. Recent work has revealed strong N IV] emission in a strong Ly α -emitting galaxy at $z = 5.6$ (Vanzella et al. 2010) and in a powerful emission-line target at $z = 3.6$ (Fosbury et al. 2003). While we do detect N IV] in 876_330 (with a flux 0.5 ± 0.2 that of C III]), we do not detect it in any of the other extreme line emitters.

Finally, many of the emission features seen in our low-luminosity sample are also often observed in narrow-lined AGNs. The AGN composite spectrum constructed in Hainline et al. (2011) suggests an average C IV EW of 16.3 Å, more than a factor of 2 larger than the most extreme sources in our sample. The narrow-line AGN composite also shows N V (5.6 Å) and He II (8.1 Å), both of which are not seen in most of the low-luminosity galaxies in our

sample. An additional point of comparison is the C IV/C III] ratio which probes the hardness of the radiation field. The average C IV/C III] flux ratio found for narrow-line AGN in the ‘class A’ composite spectrum presented in Alexandroff et al. (2013) is 7.5, more than an order of magnitude larger than most of the galaxies in our sample. Thus, while the low-luminosity systems studied in this paper may have a harder spectrum than more luminous galaxies at high redshift, they are considerably less extreme than typical narrow-lined AGNs. However, we do note that there are several narrow line AGN in the sample considered in Alexandroff et al. (2013) with C IV/C III] ratios close to those spanned by our sample (see their fig. 8), so AGN contribution cannot be discounted. In Section 5, we will explore whether the high-ionization emission features seen in Fig. 2 can be powered entirely by low-metallicity stars without requiring radiation from additional energetic sources (i.e. fast radiative shocks, X-ray binaries, AGN). Ultimately more data will be required to constrain the possible contribution of AGN.

3.4 Ly α emission of C III] emitters

The C III] emitters in our sample are almost always accompanied by powerful Ly α emission (Fig. 4a) with rest-frame EWs ranging between 50 and 150 Å (see Table 2). The link between the EW of C III] and that of Ly α was first realized through examination of $z \simeq 3$ LBG spectra in Shapley et al. (2003). By grouping galaxies by their Ly α EW, Shapley et al. (2003) demonstrated that the C III] EW increases from 0.41 to 5.37 Å as the Ly α EW increases from –14.92 (absorption) to 52.63 Å (emission).

The 17 low luminosity galaxies considered in this paper extend the results of Shapley et al. (2003) to larger Ly α and C III] EWs (Fig. 4b), confirming the close relationship between the two quantities. Our spectra generally reveal Ly α EWs in excess of 50 Å for galaxies with C III] emission EWs greater than 5 Å, similar to the largest Ly α EW bin in Shapley et al. (2003). The most extreme C III] emitters in our sample (with EWs of 10–14 Å) typically show Ly α EWs of 75–150 Å. Notably, the galaxies in our sample with the lowest EW C III] emission ($\lesssim 3$ Å) also have low equivalent Ly α emission. An exception to this relationship has recently been presented in Bayliss et al. (2014). The $z = 3.6$ galaxy presented in that paper shows numerous UV emission lines but Ly α is seen in absorption. The system is considerably more massive ($\log M^* = 9.5$) than galaxies in our sample. It is possible that large covering fractions of neutral hydrogen (and hence spectra with Ly α in absorption) might be more common among the more massive UV line emitters.

We compute the typical velocity offset between Ly α and C III] assuming a mean blended C III] rest-frame wavelength of 1907.709 Å. While our results do demonstrate that Ly α is typically redshifted with respect to C III], the velocity offsets (60–450 km s $^{-1}$ with a mean of 320 km s $^{-1}$) are slightly lower than the average value (~ 450 km s $^{-1}$) for UV-continuum-selected galaxies at $z \simeq 2$ (Steidel et al. 2010) but are comparable to Ly α -selected galaxies (e.g. Tapken et al. 2007; Hashimoto et al. 2013). We will come back to the importance of the velocity offset in Section 6.1, when assessing the case for targeting C III] in $z \gtrsim 6$ galaxies.

The tight relationship between the EW of Ly α and C III] suggests that conditions which support the efficient production and escape of Ly α radiation (i.e. low dust content, low metallicity, partial coverage of neutral hydrogen) are either directly or indirectly linked to the production of collisionally excited emission lines such as C III]. With observations indicating that Ly α becomes more common in galaxies at earlier times over the redshift range $3 \lesssim z \lesssim 6$ (Stark

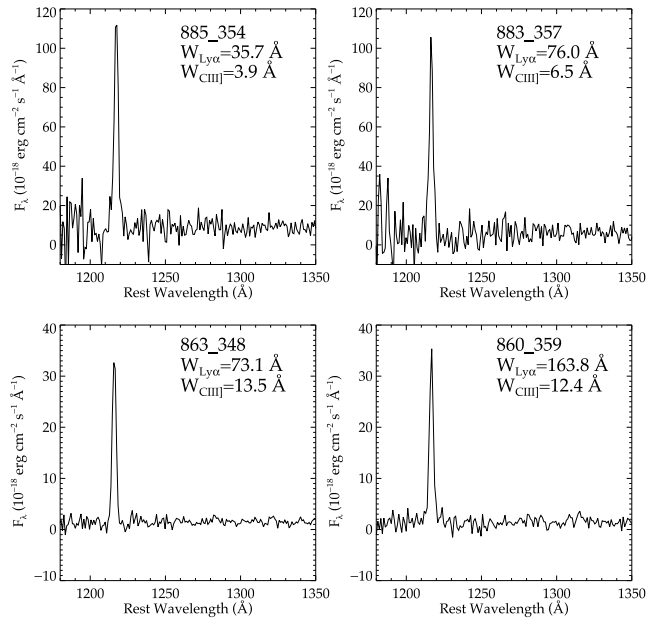


Figure 4. Ly α emission in lensed galaxies with large EW C III] emission. Left: spectra of extreme C III]-emitting galaxies at rest-frame wavelengths 1180–1350 Å. Ly α rest-frame EWs are near the maximum expected values (50–150 Å) for normal stellar populations. No sign of N v λ 1240 emission is present. Underlying continuum emission is detected with significance, but low-ionization absorption lines (Si $\pi\lambda$ 1260, OI+Si $\pi\lambda$ 1303, C $\pi\lambda$ 1334) are not detected. Right: relationship between C III] λ 1908 and Ly α EW. The low-mass lensed galaxies in our sample with Ly α and C III] measurements are denoted with red circles. We also overplot measurements for BX 418 (Erb et al. 2010) as a black triangle and for the $z \simeq 3$ composite LBG spectra (Shapley et al. 2003) as blue squares.

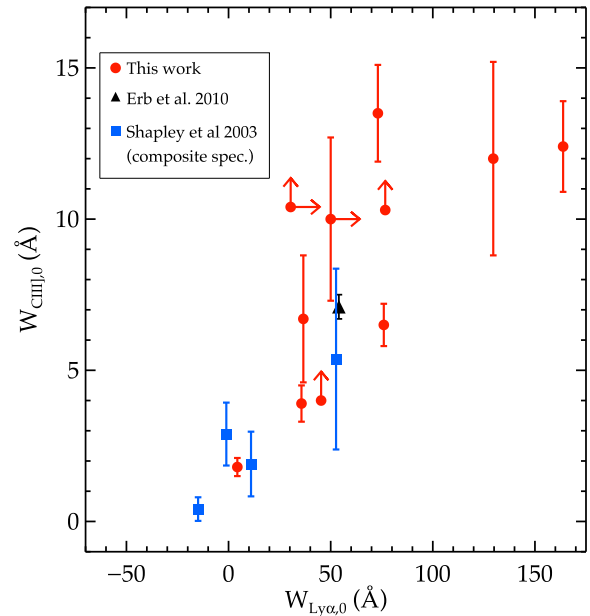
et al. 2010; Stark, Ellis & Ouchi 2011), we may expect large EW C III] emission to become ubiquitous among the galaxy population at $z \gtrsim 6$.

4 PHYSICAL PROPERTIES OF C III] EMITTERS

In this section, we seek to improve our understanding of what causes ultraviolet emission lines to have such large EWs in low-luminosity galaxies. Based on the low luminosities, we expect the ionized gas to be metal poor (see Section 4.5), elevating the electron temperature and boosting the strength of collisionally excited emission lines (O III], C III]). But other aspects of the stellar populations and gas physical conditions may contribute significantly as well. In this section, we investigate the physical properties (stellar mass, sSFR, metallicity, carbon-to-oxygen abundance) of our population of strong C III]-emitting galaxies with the goal of building a more complete picture of what might be driving the strong ultraviolet emission lines. We also investigate whether the sample of dwarf galaxies with powerful ultraviolet line emission is similar to the growing population of extreme optical-line-emitting galaxies.

4.1 Population synthesis modelling

We infer the stellar mass and sSFR of individual systems through comparison of the observed spectral energy distributions (SEDs) with population synthesis models. The procedure we adopt is similar to our earlier work (Stark et al. 2009, 2013b). We consider models with only stellar continuum and those that additionally include the contribution from nebular emission lines and continuum. The nebular line contribution at each age step is calculated from a code presented in Robertson et al. (2010). In this code, the hydrogen line intensities are computed from the case B recombination



values tabulated in Osterbrock & Ferland (2006), while the intensities of metal lines are computed using empirical results of Anders et al. (2003). The stellar continuum is computed from the models of Bruzual & Charlot (2003). For further details on the modelling procedure, see the description in Robertson et al. (2010) and Stark et al. (2013b).

For consistency with modelling of high-redshift star-forming systems with larger UV luminosities (e.g. Reddy et al. 2012b), we infer properties assuming a constant star formation history. If star formation histories of the galaxies in our sample are bursty and episodic, as motivated by many simulations of dwarf galaxies (e.g. Hopkins et al. 2013; Shen et al. 2013; Teyssier et al. 2013) and discussed in recent work on extreme emission line galaxies (EELGs; e.g. Atek et al. 2014c), our simple constant star formation history modelling will be in error. Neglecting the presence of an older stellar component from an earlier episode of star formation can cause the stellar mass to be underestimated. When two-component star formation histories including a young episode of star formation on top of an underlying very old stellar population are used in the SED fitting procedure, the inferred stellar masses of star-forming $z \simeq 2-3$ galaxies can be three times larger than derived using single-component star formation histories (e.g. Papovich, Dickinson & Ferguson 2001; Shapley et al. 2005; Dominguez et al., in preparation). In the following, we will report physical properties derived assuming single-component star formation histories (as these provide a satisfactory statistical fit to the continuum SEDs). As we acquire more measurements of rest-optical emission lines in our sample, we will explore whether simultaneous fitting of the observed continuum and emission lines (e.g. Pacifici et al. 2012) provides useful constraints on how much the current episode of star formation contributes to the total stellar mass.

We adopt a stellar metallicity of $0.2 Z_{\odot}$ for our grid (consistent with the gas-phase measurements we provide in Section 4.5) and a

Salpeter (1955) initial mass function (IMF) spanning 0.1–100 M_{\odot} . Adopting a Chabrier IMF would reduce the SFRs and stellar masses by 1.8 times. Allowing lower metallicities in the grid would not strongly affect the stellar masses (e.g. Papovich et al. 2001). Dust reddening of the stellar continuum is included following Calzetti et al. (2000). Our model grid contains SEDs with differential extinction ranging between $E(B - V)_{\text{stars}} = 0.00$ and 0.50 in steps of $\Delta E(B - V) = 0.01$. Recent work has confirmed that the extinction towards H II regions is greater than that of the stellar continuum in star-forming galaxies at high redshift (e.g. Förster Schreiber et al. 2009; Wuyts et al. 2011; Price et al. 2014), similar to measurements of star-forming galaxies in the local universe (Calzetti et al. 2000). But the extra attenuation faced by the H II regions appears to decrease with increasing sSFR (e.g. Wild et al. 2011; Price et al. 2014). The stellar continuum and nebular line emission in galaxies with very large sSFR ($\gtrsim 2.5 \text{ Gyr}^{-1}$) are found to have similar levels of attenuation at high redshift (Price et al. 2014). As we will show in Section 4.2, the continuum SEDs of galaxies in our sample imply very large sSFRs independent of assumptions about dust. Motivated by the results of Price et al. (2014), we thus assume that the nebular line and continuum attenuation is the same as the stellar continuum.

In computing the stellar masses and SFRs, we consider models with ages spanning between 30 Myr and the age of the universe at the redshift of the galaxy we are modelling. This lower age bound is often adopted based on dynamical time-scale arguments, but at lower masses, it is conceivable that younger age models might be reasonable. Reducing the minimum age (to i.e. 1–5 Myr) would introduce models with bluer intrinsic UV slopes. As a result, more reddening (and hence more star formation) would be required to fit a given observed SED. Furthermore, at very young ages for constant star formation histories, the ratio of UV luminosity and SFR has yet to equilibrate. Because of this, models with very young ages generally require much more star formation to reproduce an observed UV flux density. In the following, we will take the conservative approach of adopting a 30 Myr lower age bound, but we will also quantify the extent to which younger models would alter the inferred properties.

For each object in Table 2, we compare the galaxy SED to the model grid described above and compute the age, dust reddening, and normalization which provides the best fit to the observed SED. Using the normalization and lensing magnification factors, we derive the SFR and stellar mass from the mass-to-light ratio of the best-fitting model template. Uncertainties in the mass and SFR are derived by bootstrap resampling the observed SED within the allowed photometric errors.

4.2 Low stellar masses and large sSFRs

The stellar masses of our sample are listed in Table 5. For the 16 C III]-emitting galaxies, the SED fitting procedure (using models with nebular emission) suggests stellar masses between 2.0×10^6 and $1.4 \times 10^9 M_{\odot}$. The median stellar mass is $6.3 \times 10^7 M_{\odot}$,² roughly 65–120 times lower than that of L_{UV}^{\dagger} galaxies at $z \simeq 2-3$ (Shapley et al. 2005; Reddy & Steidel 2009; Reddy et al. 2012b) and more than a factor of 10 less massive (in stars) than BX 418, the metal-poor C III] emitter studied in Erb et al. (2010).

²If we instead use models with only stellar continuum, the stellar masses are somewhat larger for select systems (see Table 5), but the median mass ($8.1 \times 10^7 M_{\odot}$) of the C III] emitting population remains very low.

Table 5. Properties of spectroscopic sample of lensed galaxies presented in this paper. The stellar masses and SFRs are discussed in Section 4.2, and the UV continuum slopes (β) are presented in Section 4.4. We report the best-fitting stellar masses and sSFRs for models with and without nebular emission. The latter are given in parenthesis. Having only two photometric data points ($F814W$ and K_s), the SED of 854_362 does not permit determination of the UV slope, so the SFR determination assumes no dust correction.

ID	$\log(M_{\star}/M_{\odot})$	β	sSFR (Gyr^{-1})	$W_{[\text{O III}]+\text{H}\beta}$ (\AA)
MACS 0451				
1.1	7.69(7.80)	−2.7	28(35)	–
6.2	9.00(9.12)	−1.2	23(35)	–
4.1	7.51(7.58)	−1.5	34(34)	–
3.1	7.77(8.09)	−2.2	27(4.1)	–
Abell 68				
C4	7.79(7.84)	−2.7	18(19)	–
C20b	6.63(6.69)	−2.3	23(20)	–
Abell 1689				
881_329	6.30(6.54)	−2.5	10(5.8)	6230 ± 3610
899_340	8.19(8.27)	−1.7	23(27)	110 ± 60
883_357	8.12(8.15)	−2.0	24(21)	660 ± 40
860_359	8.06(8.17)	−1.8	4.0(5.2)	1550 ± 150
885_354	8.21(8.26)	−1.8	31(34)	720 ± 40
863_348	7.46(7.57)	−2.0	35(35)	1620 ± 110
876_330	7.80(7.83)	−2.2	4.8(5.9)	740 ± 190
869_328	6.71(6.87)	−2.8	31(27)	–
854_344	8.91(9.01)	−1.8	35(35)	–
854_362	9.15(9.09)	–	34(47)	–
846_340	8.97(8.86)	−2.9	1.9(3.0)	–

Our spectra indicate that (similar to BX 418) the physical conditions in many star-forming galaxies with stellar masses between 10^6 and $10^8 M_{\odot}$ are particularly conducive to the production of large EW collisionally excited lines. Based on the presence of C III] emission among more massive ($\simeq 10^9 M_{\odot}$) galaxies in our sample (854_362) and elsewhere in the literature (Shapley et al. 2003; Erb et al. 2010; Christensen et al. 2012a,b; Stark et al. 2013a), we suspect that low stellar mass is not the dominant factor regulating the strength of collisionally excited emission lines. More likely the connection between low stellar mass and C III] emission is indicative of the dependence of yet more important properties (i.e. metallicity) on stellar mass.

Examination of existing samples in the literature suggests that the sSFR might also be an important indicator of large EW C III] emission. For example, while the masses of M2031 ($1.4 \times 10^9 M_{\odot}$; Christensen et al. 2012a) and BX 418 ($0.9 \times 10^9 M_{\odot}$ for assumed Chabrier IMF; Erb et al. 2010) are not nearly as low as many of the galaxies in our sample, their C III] EWs are comparable. In addition to having low metallicities, both galaxies stand out as having unusually large sSFRs (17 Gyr^{-1} for BX 418 and 13 Gyr^{-1} for M2031) among galaxies with moderate ($\sim 10^9 M_{\odot}$) stellar masses.

Similar to BX 418 and M2031, the sSFRs of the extreme C III] emitters in our sample are very large. The median value determined from the continuum SEDs, 27 Gyr^{-1} , is more than 10 times that of typical $z \simeq 2-3$ UV-selected galaxies (e.g. Reddy et al. 2012b), indicating that the dwarf galaxies with powerful line emission have undergone a phase of unusually rapid stellar mass growth over the past 100 Myr (the time-scale probed by the UV continuum

luminosity).³ Galaxies caught in the midst of such an upturn in their star formation might be expected to exhibit prominent nebular emission lines for a variety of reasons. First, the reservoir of ionizing radiation per unit mass will be greater during such an active period of star formation, causing an enhanced ionization parameter. Secondly, the ionizing continuum is likely to be somewhat harder at young ages, translating into a larger electron temperature and stronger collisionally excited lines. In future, it should be possible to confirm the connection between sSFR and UV lines through a comparison of the H α EW (a proxy for the sSFR over the last 10 Myr) and the C III] EW.

But the inference of a very large sSFR from a broad-band SED does not guarantee extreme EW UV emission lines. For example, the sSFR of the only galaxy in our sample without a C III] detection (MACS 0451-6.2) is between 23 and 35 Gyr⁻¹, comparable to many of the UV-line-emitting galaxies in our sample. Clearly, factors other than the sSFR (i.e. metallicity, dust content) play an important role in regulating the EW of the UV emission lines.

An additional complication in using the derived sSFR as an indicator of whether or not a galaxy is likely to be an extreme UV line emitter is that the UV continuum (which we used to derive the SFR) only reflects activity on 100 Myr time-scales. If star formation has fallen off significantly in the past ~ 10 Myr (as might be expected if star formation is bursty), then the sSFR derived from the stellar continuum might still be large, but the hot stars required to power nebular emission lines would be mostly absent. As we will argue in Section 4.4, this is a possible explanation for the weak nebular line emission in 869_328, a very low stellar mass galaxy with a continuum-derived sSFR between 27 and 31 Gyr⁻¹.

4.3 Extreme [O III]+H β EWs

Recent studies have identified a population of galaxies at high redshift with very large rest-optical EW ($\gtrsim 500$ – 1000 Å) emission lines. There is now emerging evidence that such extreme (rest-optical) emission line galaxies (EELGs) become substantially more common at higher redshifts (e.g. Shim et al. 2011; Stark et al. 2013b; Smit et al. 2014). The latest results at $z \gtrsim 6$ (Labbé et al. 2013; Smit et al. 2014) indicate that most early star-forming galaxies have extremely large EW rest-optical emission lines.

Since the physics of collisionally excited emission lines is essentially the same in the ultraviolet and optical, it seems likely that the physical conditions (i.e. metallicity, sSFR) which cause the extreme optical line emission in EELGs are identical to those responsible for the prominent UV emission lines in our sample of lensed galaxies. If this is the case, we should expect the galaxies in our sample to exhibit [O III] $\lambda 5007$ emission lines with EWs similar to the population of EELGs. Given the ubiquitous presence of large EW rest-optical line emission in galaxies at $z \gtrsim 6$, empirical evidence demonstrating a firm connection between the EELG population and our extreme rest-UV-line-emitting galaxies would help build the case that rest-UV lines such as C III] will be present in the spectra of $z \gtrsim 6$ galaxies.

³This average is based on modelling with a minimum age of 30 Myr. As discussed in Section 4.1, lowering the minimum age will tend to increase the inferred SFR. If we were to adopt 5 Myr as the lower age threshold, we would find a median sSFR of 32 Gyr⁻¹. As noted in Section 4.1, the stellar masses could be underestimated by a factor of 2–3 if an underlying old stellar component is hidden by the current episode of star formation powering the extreme line emission. But even in this case, the sSFRs are still well above average (e.g. Reddy et al. 2012b).

While efforts to measure the rest-optical emission lines of our intermediate-redshift sample with near-infrared spectroscopy are now underway (Section 4.5), many of the extreme C III] emitting galaxies are at redshifts which place their rest-optical emission lines in regions of low atmospheric transmission and are thus difficult to characterize from the ground. However, if the galaxies in our sample have extremely large rest-optical EWs, we should see prominent flux excesses in the *HST* WFC3/IR broad-band filters which contain the emission lines. In our previous work (Stark et al. 2013b; Schenker et al. 2013b) and that of other groups (e.g. van der Wel et al. 2011; Smit et al. 2014), it has become customary to use the observed flux excesses in specific redshift intervals to characterize rest-optical line emission-line EWs.

We will focus our rest-optical line analysis on galaxies in the Abell 1689 field. With deep WFC3/IR imaging in four filters (Y_{105} , J_{125} , J_{140} , H_{160}), we can identify large EW [O III] emission via its influence on the flux density in either the J_{125} band (for galaxies at $1.18 < z < 1.80$), the J_{140} band ($1.38 < z < 2.20$), or the H_{160} band ($1.78 < z < 2.37$). Throughout much of these redshift intervals, the observed flux excesses will also be affected by H β emission, and hence the inferred EWs will reflect the [O III]+H β line strengths. Seven of the C III] emitters towards Abell 1689 fall in one of the redshift intervals noted above. It is immediately clear from examination of the SEDs in Fig. 5 that the observed flux in the bandpasses which are contaminated by [O III]+H β are substantially in excess of that expected from stellar continuum emission. Following the techniques we used in Stark et al. (2013b), we compute the line flux and EW required to produce the flux excess.

The median (rest-frame) [O III]+H β EWs required to explain the flux excess is 740 Å (Table 4). Six of seven galaxies in the appropriate redshift window have inferred rest-frame [O III]+H β EWs in excess of 660 Å, similar to many of the rest-optically selected EELGs at similar redshifts (e.g. Atek et al. 2011; van der Wel et al. 2011; Maseda et al. 2013). The physical link between the UV and optical line emitters is not surprising, as we outlined above. If the ubiquity of large EW optical emission lines is confirmed with larger samples at $z \gtrsim 4$ (e.g. Holden et al. 2014; Labbé et al. 2013; Schenker et al. 2013b; Stark et al. 2013b; Smit et al. 2014), the connection would bolster confidence that ultraviolet emission lines such as C III] or O III] might be visible in suitably deep spectroscopic exposures.

4.4 Blue UV continuum slopes

The UV-continuum slope (parametrized as β where $f_{\lambda} \propto \lambda^{\beta}$) provides a unique constraint on the dust extinction in high-redshift UV-selected galaxies (e.g. Reddy et al. 2012a) and is additionally affected by the metallicity and age of the stellar population. Over the last several years, considerable effort has been focused on determining the distribution of UV-continuum slopes in galaxies at very high redshifts (e.g. Wilkins et al. 2011; Bouwens et al. 2012, 2013; Finkelstein et al. 2012; Dunlop et al. 2013; Rogers, McLure & Dunlop 2013). These studies reveal that $z \approx 7$ galaxies have blue UV slopes ($\beta \approx -2.0$ to ≈ -2.5), consistent with minimal dust reddening. Comparison to lower redshift samples reveals mild-redshift evolution, with galaxies at $z \approx 7$ bluer than those of similar UV luminosity at $z \approx 2.5$ by $\Delta\beta \approx 0.3$ (Bouwens et al. 2013). While some controversy remains at the highest redshifts, the UV slopes show a trend towards bluer colours at lower UV luminosities in galaxies at $z \approx 4$ – 5 (e.g. Wilkins et al. 2011; Bouwens et al. 2013), as would be expected if low-luminosity galaxies are metal poor with little reddening from dust.

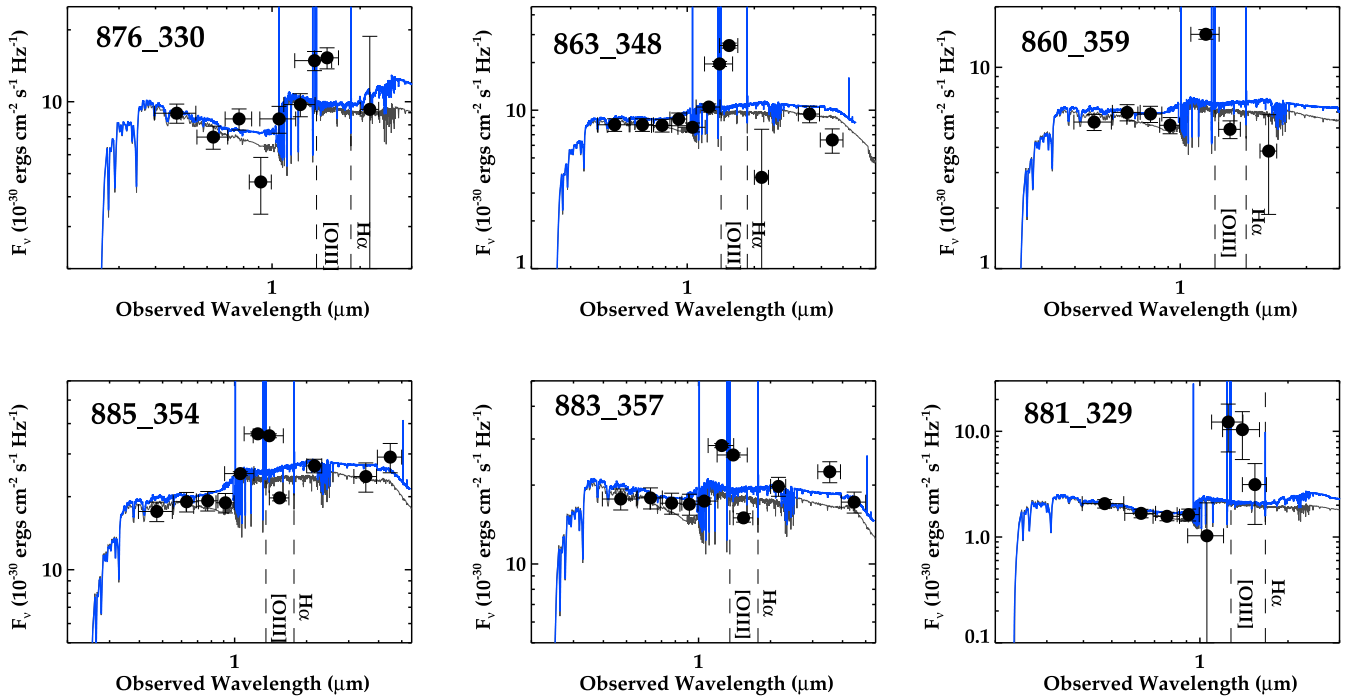


Figure 5. Evidence for large EW rest-optical [O III]+H β emission in C III] emitters. The impact of [O III]+H β emission is clearly seen on the near-infrared broad-band photometry. The dashed lines denote the observed wavelengths of [O III] λ 5007 and H α . We show the best-fitting population synthesis models with stellar continuum and nebular emission in blue. The best-fitting models with only stellar continuum (grey) provide a much poorer fit to the observations. The [O III]+H β EWs required to explain the observed flux excesses are typically in excess of 660 Å rest frame (see Table 4).

Here, we measure the UV slopes of our lensed galaxy sample and investigate whether there is a connection with the EW of C III] emission. UV slopes are derived using the flux information from filters spanning rest-frame wavelengths of 1300 and 2500 Å. Given the spread of redshifts within our sample (and the different filter deployment in the three cluster fields), the exact filters used vary from galaxy to galaxy. We take care to exclude filters which are affected by the Ly α forest or Ly α emission. The metal UV lines do not have large enough EW to significantly affect the broad-band flux measurements. UV slopes are derived for each source in our spectroscopic sample using a simple least squares minimization procedure.

The UV slopes are provided in Table 5. The median value ($\beta \simeq -2.2$) is considerably bluer than that of more luminous systems at similar redshifts (e.g. Reddy et al. 2012a), likely reflecting the reduced dust content, lower metallicities, and younger ages of the low-luminosity galaxies in our sample. Comparison of our sample with the more luminous systems in Shapley et al. (2003) reveals that galaxies with blue colours ($\beta \lesssim -2$) do tend to have larger EW C III] emission than galaxies with redder UV slopes ($\beta \gtrsim -1.3$). The importance of UV slope as an indicator of C III] EW is made evident by MACS 0451-6.2, the only galaxy in our sample without C III] emission. While its sSFR is as large as many of the most prominent line emitters that we consider in this paper, MACS 0451-6.2 stands out as the reddest galaxy ($\beta = -1.2$) in our sample. As is evident from Fig. 6, the red UV colour places MACS 0451-6.2 in a regime where C III] EWs are generally very low.

The dependence of C III] EW on UV colour is to be expected. Galaxies with UV slopes bluer than $\beta \sim -2$ (indicative of little to no reddening from dust) are likely to be reasonably metal poor. Given the larger electron temperatures associated with ionized gas in galaxies with moderately low metallicities (see Section 4.5 for

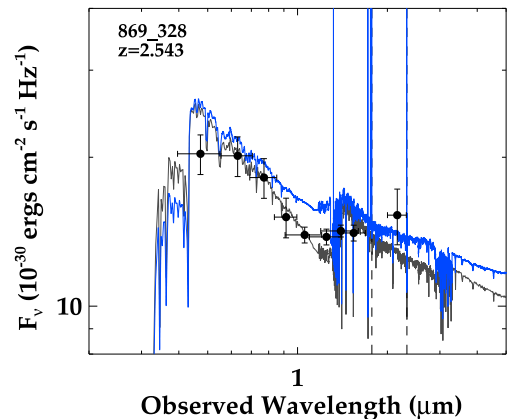


Figure 6. Example of low stellar mass ($5.1 \times 10^6 M_{\odot}$) galaxy in our sample with low EW UV nebular emission lines ($W_{\text{C III]}} = 1.8 \text{ \AA}$). The best-fitting stellar continuum (dark grey) and nebular+stellar models (blue) are overlaid. The broad-band SED is among the bluest in our sample ($\beta = -2.8$) and the sSFR reveals significant stellar mass growth in the past 100 Myr. The UV slope of the best-fitting nebular+stellar model is considerably redder than observed owing to nebular continuum emission. The stellar continuum models provide a much better fit to the data.

more discussion), star-forming systems with very blue UV colours are prime candidates for having large EW emission lines in the ultraviolet and optical. The low dust covering fraction of galaxies with very blue UV colours may also play an important role. If H II regions are more strongly attenuated than the stellar continuum emission (see discussion in Section 4.1), then the EWs of UV emission lines will be weakened in galaxies with reddened continuum.

Given that the UV continuum slope is one of the few quantities that can be measured at $z \gtrsim 7$, the relationship between colour and C III] EW will be crucial for assessing the feasibility of pursuing C III] in reionization-era galaxies and will provide a useful baseline for interpreting the results. With most of the star-forming population at $z \gtrsim 7$ exhibiting blue UV slopes, it seems likely that large EW C III] emission should be much more common in early star-forming galaxies.

But as is clear from the scatter in the UV slopes in Table 5, galaxies with blue UV colours do not always have extreme UV line emission. This point is nicely illustrated by the spectrum of 869_328, one of the lowest stellar mass ($5.1 \times 10^6 M_{\odot}$) galaxies in our sample. While the UV slope of 869_328 is among the bluest in our sample ($\beta \simeq -2.8$), the EW of C III] (1.8 Å) and Ly α (4.3 Å) are both found to be very low (although there is extended Ly α emission spanning $\simeq 25$ arcsec). As is clear from the SED (Fig. 6), this galaxy appears very young, with an sSFR of between 27 and 31 Gyr $^{-1}$. Galaxies with such large sSFR are commonly accompanied by very prominent nebular emission. But the nebular + stellar continuum model struggles to reproduce the observed SED. Not only are the emission lines much weaker than expected, but the impact of nebular continuum causes the UV slope of the best-fitting model (blue curve overlaid in Fig. 6) to be considerably redder than observed.

The physical origin of the weak nebular line and nebular continuum emission in 869_328 is not clear. One possibility is that the bulk of the ionizing radiation is escaping the galaxy. It is also possible that the massive O and early B stars required to power nebular emission are mostly absent. Such a situation could occur from bursty star formation or stochastic sampling of the IMF. In the local volume, the lowest luminosity star-forming galaxies often exhibit very low ratios of H α to far-UV continuum (e.g. Lee et al. 2009). It is conceivable that 869_328, one of the lowest mass galaxies in our sample, is part of an analogous population at high redshift. But clearly some caution must be exercised in interpreting this target given the limited nature of the data in hand. Rest-optical emission lines (in particular H α) will soon provide a considerably more reliable picture of the nature of this source.

4.5 Low gas-phase metallicity

As we emphasized at the outset of Section 4, the gas-phase metallicity plays an important role in governing the strength of UV emission lines such as C III] and O III]. The large electron temperature that arises due to inefficient cooling in moderately low metallicity gas tends to increase the EW of collisionally excited emission lines, while the harder ionizing output from low-metallicity stellar populations is likely to boost the output of ionizing photons. Perhaps not surprisingly, the low-mass star-forming galaxies known at high redshift with large EW C III] emission (e.g. Erb et al. 2010; Christensen et al. 2012b; James et al. 2014) tend to have optical emission-line ratios consistent with moderately metal poor ($\lesssim 0.2 Z_{\odot}$) ionized gas (an exception is the C III] emitter reported in Bayliss et al. 2014 with $0.5 Z_{\odot}$). Here, we characterize the gas-phase chemical abundances of a small subset of galaxies in our sample.

4.5.1 Characterization of optical emission lines

We calculate nebular redshifts and line fluxes through Gaussian fits to the emission lines detected with FIRE and XSHOOTER. To determine the uncertainty in the line fluxes and redshifts, we generate 1000 realizations of the spectra by perturbing the flux

at each wavelength by an amount consistent with the error spectrum. We fit the line fluxes and redshifts of each of the mock spectra. The standard deviation of the flux and redshift distribution is then used to compute 1σ uncertainties in each of these quantities. In the remainder of this subsection, we provide brief descriptions of the emission lines detected in each of the five galaxies targeted.

The XSHOOTER spectrum of 860_359 shows strong emission from H β , [O III] $\lambda 4959$, [O III] $\lambda 5007$, and H α (see Amanullah et al. 2011). Line fluxes are listed in Table 6. The flux ratio of H α and H β (3.0 ± 0.1) suggests that the rest-optical emission lines are not strongly reddened by dust. The redshift of the galaxy places [O III] $\lambda 5007$ at an observed wavelength (1.353 μm) strongly attenuated by telluric absorption. While the line is significantly detected, the flux measurement is fairly uncertain owing to the low atmospheric transmission. We thus infer the [O III] $\lambda 5007$ flux using our measurement of [O III] $\lambda 4959$ (which is located at a wavelength less strongly attenuated by telluric absorption) and the theoretical [O III] 5007/4959 flux ratio (set by statistical weights) of 2.98. [N II] $\lambda 6584$ is not detected with significance. A 2σ upper limit is listed in Table 6. The [O II] emission line is in a noisy region of the XSHOOTER spectrum (in between the peak sensitivity of the visible and near-infrared arm) resulting in coarse upper limits on the flux.

MACS 0451-1.1 was observed with FIRE on 2012 February 16 and October 29. The 2012 February 16 observation of MACS 0451-1.1 was oriented perpendicular to the extended arc to ensure optimal sky subtraction (similar to the VLT/FORS orientation), covering only the central region. The position angle (PA) adopted on 2012 October 29 was chosen to include a larger fraction of the lensed galaxy. In both spectra, we confidently detect H α , [O III] $\lambda 4959$, and [O III] $\lambda 5007$ (Fig. 7; see Table 6 for flux measurements). Sky subtraction residuals prevent useful constraints on [N II] $\lambda 6584$, and [O II] is not detected. We see H β confidently in the 2012 October 29 spectrum. The flux ratio of H α and H β (2.6 ± 0.3) suggests that the emission lines are not strongly affected by reddening. In the 2012 February 16 spectrum, the formal significance of the H β detection is much lower ($S/N = 1.6$). Rather than introducing a noisy H β measurement into analysis of the 2012 February 16 spectrum, we follow the approach taken in similar cases (e.g. Hainline et al. 2009) of estimating the H β flux by adjusting the measured H α flux assuming the ratio for case B hydrogen recombination and accounting for reddening based on the $E(B - V)$ inferred from the SED. We assume an intrinsic H α /H β ratio of 2.81 (the average of the case B ratios expected for gas with $T_e = 1.0 \times 10^4$ K and 2.0×10^4 K; Osterbrock 1989) and assume no reddening. The estimated value is listed in Table 6.

The near-IR spectrum of MACS 0451-6.2 reveals detections of many of the strongest rest-optical emission lines (Fig. 7) including [O II], H β , [O III], and H α . The [N II] $\lambda 6584$ emission line is at the edge of a sky line but is significantly detected. By fitting the half of the line which is unaffected by sky residuals, we infer a total line flux of 3.1×10^{-17} erg cm $^{-2}$ s $^{-1}$. We also detect a faint emission feature at the location of [N II] $\lambda 6548$ with a line flux of 9.2×10^{-18} erg cm $^{-2}$ s $^{-1}$. Assuming an [N II] 6583/6548 doublet flux ratio of 2.93 (as set by the statistical weights of the energy levels), we derive an [N II] $\lambda 6584$ flux of 2.7×10^{-17} erg cm $^{-2}$ s $^{-1}$. We use the mean value of the two [N II] $\lambda 6584$ flux estimates in Table 6. The measured Balmer decrement (H α /H $\beta \simeq 3.6$) indicates that dust reddening moderately affects the rest-optical emission-line flux ratios (consistent with a selective extinction of $E(B - V)_{\text{gas}} = 0.20$ following Calzetti et al. 2000) as expected based on the red UV continuum slope ($\beta \simeq -1.2$) inferred from the SED.

Table 6. Rest-optical emission-line flux in units of 10^{-17} erg cm^{-2} s^{-1} . In cases where no emission is detected, we list 2σ upper limits. The fluxes listed above do not include the fraction of the lensed galaxy which is not sampled by the slit. MACS 0451-1.1 was observed using two separate PAs with Magellan/FIRE. The epoch 1 observations (2012 February 16) are denoted 1.1a while the epoch 2 observations (2012 October 29) are listed as 1.1b. Emission lines flagged with a dagger symbol (\dagger) are indirect measurements owing to sky subtraction residuals, telluric absorption, or low S/N; for details, see Section 4.5.1.

	MACS 0451 1.1a	MACS 0451 1.1b	MAC S0451 6.2	MACS 0451 3.1	Abell 1689 899_340	Abell 1689 860_359
z_{neb}	2.0596	2.0596	1.4048	1.9043	1.5996	1.7024
$F_{[\text{O II}]\lambda 3726}$	<0.6	<0.6	2.5 ± 0.7	<0.9	<3.1	<1.9
$F_{[\text{O II}]\lambda 3729}$	–	<0.6	3.2 ± 1.0	<1.1	<3.7	<1.7
$F_{\text{H}\beta}$	$1.3\dagger \pm 0.5$	1.9 ± 0.2	4.9 ± 0.4	–	<2.5	3.1 ± 0.1
$F_{[\text{O III}]\lambda 4959}$	2.9 ± 0.1	2.6 ± 0.1	5.1 ± 0.3	–	–	6.3 ± 0.1
$F_{[\text{O III}]\lambda 5007}$	7.8 ± 0.2	7.5 ± 0.1	13.7 ± 0.5	3.1 ± 0.4	9.0 ± 1.2	$18.6\dagger \pm 0.1$
$F_{\text{H}\alpha}$	3.6 ± 0.2	4.9 ± 0.3	17.7 ± 0.3	–	7.0 ± 0.9	9.2 ± 0.1
$F_{[\text{N II}]\lambda 6584}$	–	–	$2.9\dagger \pm 0.3$	–	–	$\lesssim 0.2$

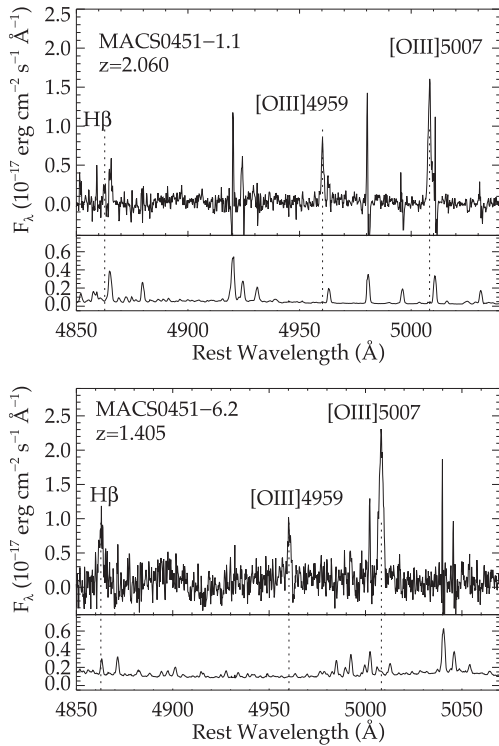


Figure 7. Magellan/FIRE near-infrared spectrum of MACS 0451-1.1 (top panel) and MACS 0451-6.2 (bottom panel). The 1σ noise spectrum is presented underneath the object spectrum in both panels. Emission-line fluxes are listed in Table 6.

The final two galaxies remaining in Table 6 are MACS 0451-3.1 and 899_340. The FIRE spectrum of MACS 0451-3.1 contains strong $[\text{O III}]\lambda 5007$ emission, indicating a nebular redshift of $z = 1.9043$. At this redshift, most of the other strong rest-optical emission lines are in regions of low atmospheric transmission and are not detected. The FIRE spectrum of 899_340 exhibits $[\text{O III}]\lambda 5007$ and $\text{H}\alpha$, indicating a nebular redshift of $z = 1.600$. Both $[\text{O III}]\lambda 4959$ and $[\text{N II}]\lambda 6584$ are obscured by sky lines. The $[\text{O II}]$ and $\text{H}\beta$ lines are located in clean regions but are not detected. Line fluxes (and 2σ upper limits) are listed in Table 6.

4.5.2 Metallicity estimates

The rest-optical emission lines discussed in Section 4.5.1 allow us to constrain the gas-phase metallicity of three galaxies (MACS 0451-1.1, MACS 0451-6.2, 860_359) in our sample. Since the spectra are not deep enough to detect the electron temperature (T_e) sensitive $[\text{O III}]\lambda 4363$ emission line, we estimate oxygen abundances using standard strong-line abundance indicators based on the relative strength of strong collisionally excited emission lines ($[\text{O II}]$, $[\text{O III}]$, $[\text{N II}]$) and hydrogen recombination lines ($\text{H}\alpha$, $\text{H}\beta$) in the rest-frame optical. In the following, we will consider the R_{23} index ($R_{23} \equiv ([\text{O II}] + [\text{O III}]) / \text{H}\beta$), the N2 index ($\text{N2} \equiv \log\{[\text{N II}]\lambda 6584 / \text{H}\alpha\}$), and the O3N2 index ($\text{O3N2} \equiv \log\{([\text{O II}]/\text{H}\beta) / ([\text{N II}]/\text{H}\alpha)\}$). While each of these indices can provide an estimate of the oxygen abundance, there are systematic offsets in the absolute abundance scales of the different calibrations. We account for these using the conversions presented in Kewley & Ellison (2008). To reliably map these strong line indicators to an oxygen abundance, care must be taken to assess the ionization state of the gas. This is usually done through constraining the ionization parameter, U , defined as the ratio of the surface flux of hydrogen ionizing photons and density of hydrogen atoms. For this purpose, we will also calculate the ratio of the $[\text{O III}]$ and $[\text{O II}]$ lines ($\text{O}_{32} \equiv \{[\text{O III}]\lambda 4959 + [\text{O III}]\lambda 5007\} / [\text{O II}]\lambda 3727$).

We will make use of the Pettini & Pagel (2004, hereafter PP04) calibration of the N2 and O3N2 index. For the R_{23} index, we follow the iterative approach discussed in Kobulnicky & Kewley (2004, hereafter KK04), which is based on calibrations derived from the photoionization models of Kewley & Dopita (2002). The R_{23} index is well known to be double valued with metallicity, requiring external constraints to establish whether the galaxy is low metallicity (and thus on the ‘lower branch’) or high metallicity (on the ‘upper branch’). For each galaxy we consider below, we will discuss whether the upper branch or lower branch is appropriate. As discussed above, the relationship between the measured R_{23} value and the oxygen abundance, O/H , is dependent on the ionization parameter. While the O_{32} diagnostic constrains the ionization parameter, the relationship between the two quantities depends on the metallicity. We therefore must adopt an iterative scheme to ensure convergence in U and O/H . Using equation 13 of KK04, we calculate U from our measurement of O_{32} and an initial guess at O/H . We then derive the oxygen abundance by inputting the inferred ionization parameter and measured R_{23} index into the lower or upper branch R_{23} calibration of KK04. If the final inferred metallicity is significantly

different from our initial guess, we re-do the calculation inserting the derived value of O/H into the ionization parameter calculation. Several cycles are typically required before convergence is reached.

The first system we consider is 860_359, one of the extreme C III]-emitting galaxies in our sample. Based on the flux ratios in Table 6, we measure $N2 < -1.7$ and $O3N2 > 2.4$. Following the calibrations of PP04, these measurements suggest an oxygen abundance of $12 + \log O/H < 7.9$ for N2 and O3N2. Assuming the solar abundance value of $12 + \log O/H = 8.66$ (Asplund et al. 2009), these observations suggest that the typical metallicity is less than $0.2 Z_{\odot}$. The ratio of [N II] and H α places the galaxy on the lower branch of the R_{23} -O/H relationship (see e.g. KK04). Taking into consideration the 2σ limit on the [O II] flux, we find $8.0 < R_{23} < 9.2$ and $O_{32} > 6.9$. Applying the iterative KK04 procedure described above, we find that these constraints translate into an upper limit on the oxygen abundance of $12 + \log O/H < 8.3$. Applying the mapping derived in Kewley & Ellison (2008), we find that the KK04 abundance limit corresponds to $12 + \log O/H < 8.2$ on the PP04 N2 abundance scale. Both calibrations suggest that the ionized gas in 860_359 is moderately metal poor with an oxygen abundance no greater than $0.2\text{--}0.3 Z_{\odot}$.

The second system we examine is MACS 0451-1.1, a moderate EW C III] emitter with low stellar mass ($4.9\text{--}6.3 \times 10^7 M_{\odot}$), large sSFR ($28\text{--}35 \text{ Gyr}^{-1}$), and blue UV slope ($\beta = -2.7$). As explained in Section 4.5.1, the galaxy was observed with two different PAs with FIRE. The non-detection of [O II] in both epochs bounds the R_{23} index to the range $8.4\text{--}9.3$ (2012 February 16) and $5.3\text{--}5.9$ (2012 October 29). We find that $O_{32} > 8.9$ (2012 February 16) and $O_{32} > 8.4$ (2012 October 29). Based on the Balmer decrement measurement (see discussion in Section 4.5.1), we do not apply reddening corrections to the line ratios. Without a robust measurement on [N II], we cannot reliably place MACS 0451-1.1 on the upper or lower branch. However, most available evidence for MACS 0451-1.1 (low luminosity, low stellar mass, blue UV continuum slope, detection of T_e -sensitive line O III] $\lambda 1666$ emission line) suggests that the galaxy resides on the lower branch. Following the iterative KK04 approach (and considering a range of O_{32} and R_{23} values consistent with our [O II] flux limit), we find $12 + \log O/H \lesssim 8.0$ (2012 October 29) and $12 + \log O/H \lesssim 8.3$ for (2012 February 16). In the more unlikely case that MACS 0451-1.1 lies on the upper branch, the KK04 parametrization implies $12 + \log O/H \gtrsim 8.8$ (2012 October 29) and $12 + \log O/H \gtrsim 8.5$ (2012 February 16).⁴ The differences in the metallicities between the two epochs may reflect physical differences in the oxygen abundance probed by the two slit positions. Integral field observations are required to reliably map the metallicity gradient and investigate whether shocks or AGN might drive line ratio variations across the galaxy (e.g. Jones et al. 2013; Yuan, Kewley & Rich 2013). But regardless of the variation in metallicity across the source, the integrated measurements derived here suggest that the ionized gas in MACS 0451-1.1 is likely to be moderately metal poor ($\lesssim 0.2\text{--}0.4 Z_{\odot}$).

The third and final galaxy we examine is MACS 0451-6.2. As we have already discussed, MACS 0451-6.2 has no detectable C III] emission and is a reasonably massive ($1.2 \times 10^9 M_{\odot}$ in stars) and

red ($\beta = -1.2$) galaxy for our sample. The relative fluxes of [N II], H α , and [O III] $\lambda 5007$ indicate that $N2 = -0.8$ and $O3N2 = 1.7$. Using the PP04 calibration, we derive oxygen abundances of $12 + \log (O/H) = 8.4$ and 8.3 from the N2 and O3N2 calibrations, respectively. Again applying the Kewley & Ellison (2008) conversions, we find that these abundances correspond to $12 + \log (O/H) = 8.8$ and 8.7 on the KK04 abundance scale. The measured N2 value places this galaxy on the upper branch of the R_{23} -O/H relationship. Without any reddening correction, we find that $R_{23} = 5.0$. After correcting the line fluxes for reddening, we derive a slightly larger value of $R_{23} = 5.2$. Following the KK04 iterative procedure described above (although now using the upper branch calibration), we infer an oxygen abundance of $12 + \log (O/H) = 8.8$ from the de-reddened flux ratios, consistent with expectations from the N2 and O3N2 indices.

The metallicity estimates calculated above are consistent with the general picture proposed at the outset of Section 4. The two galaxies considered above with large EW C III] emission appear to have moderately metal poor ($\lesssim 0.2\text{--}0.4 Z_{\odot}$) gas. At these metallicities, the electron temperature of ionized gas is elevated, increasing the strength of collisionally excited lines. Prominent line emission is likely less common in more metal-rich galaxies. Indeed, the metallicity of the only galaxy in our sample without C III] emission (MACS 0451-6.2) is noticeably larger ($0.4\text{--}0.5 Z_{\odot}$ on the PP04 scale) than that of the low-luminosity galaxies with C III] detections.

4.6 Gas-phase C/O ratio

For C III] to be a viable redshift indicator at $z \gtrsim 6$, carbon must be deposited into the ISM on reasonably short time-scales. While the presence of large EW [O III]+H β emission in $z \simeq 7\text{--}8$ galaxies (e.g. Labbé et al. 2013; Smit et al. 2014) requires a non-negligible gas-phase abundance of oxygen at early times, it could take much longer for carbon to reach the abundance required to produce prominent C III] emission. Before we can reliably motivate the use of C III] as a probe of $z \gtrsim 6$ galaxies, we must therefore understand the physics regulating the relative abundance of carbon and oxygen in the ionized gas of early star-forming systems.

Studies of the carbon-to-oxygen (C/O) ratio in galactic stars (Bensby & Feltz 2006; Fabbian et al. 2009), nearby H II regions (e.g. Garnett et al. 1995, 1997, 1999; Kobulnicky & Skillman 1998), damped Ly α emitters (Cooke et al. 2011), and high-redshift galaxies (Shapley et al. 2003; Erb et al. 2010) demonstrate that the C/O ratio increases with increasing O/H for $12 + \log(O/H) > 7.7$. As discussed at length in earlier studies, the physical origin of this trend is likely associated with the metallicity dependence of winds from massive rotating stars, along with the delayed release of carbon from lower mass stars (e.g. Henry, Edmunds & Koumlypen 2000; Akerman et al. 2004).

Given the low metallicity of dwarf galaxies in our sample (Section 4.5), the framework described above suggests that carbon is likely to be substantially underabundant with respect to oxygen. We can quantify the C/O ratio by constraining the flux ratio of O III] $\lambda\lambda 1661, 1666$ to C III] $\lambda\lambda 1907, 1909$ (e.g. Garnett et al. 1995; Shapley et al. 2003; Erb et al. 2010). We will use the recent parametrization presented in Erb et al. (2010):

$$\frac{C^{+2}}{O^{+2}} = 0.15e^{-1.054/t} \frac{I(C\text{ III]}\lambda\lambda 1907, 1909)}{I(O\text{ III]}\lambda\lambda 1661, 1666)}, \quad (1)$$

where $t = T_e/10^4$ K. The next step is to convert the measured C^{+2}/O^{+2} ratio to a C/O ratio. Since O^{+2} has a higher ionization potential than C^{+2} (54.9 eV versus 47.9 eV), carbon will be triply

⁴Using the relations presented in Kewley & Ellison (2008), we convert the KK04 oxygen abundances to the absolute abundance scale of the PP04 N2 calibration. The lower branch measurements are similar for both calibrations. But we find that the upper branch abundance metallicities are slightly lower on the PP04 N2 scale: $12 + \log O/H \gtrsim 8.4$ (2012 October 29 spectrum) and $12 + \log O/H \gtrsim 8.2$ (2012 February 16 spectrum).

ionized while oxygen is still primarily in the O^{+2} state. Hence, an observed trend towards lower C^{+2}/O^{+2} ratios may result from either an increase in the ionizing flux or a reduction in the C/O ratio. To break this degeneracy, we must account for the ionization state of the gas. This is done by multiplying the observationally inferred C^{+2}/O^{+2} ratio by an ionization correction factor (ICF) defined as the ratio of the volume fractions of oxygen in O^{+2} and carbon in C^{+2} :

$$\frac{C}{O} = \frac{C^{+2}}{O^{+2}} \times \text{ICF}. \quad (2)$$

The ICF can be inferred through constraints on the ionizing spectrum through ionization parameter diagnostics such as O_{32} . Using a suite of CLOUDY v08.00 photoionization models (Ferland et al. 1998), Erb et al. (2010) demonstrated that for stellar populations with ionization parameters in the range $-2.5 \lesssim \log U \lesssim -2.0$, the ICF is close to unity. As the ionization parameter increases to $\log U \simeq -1.0$, the ICF is predicted to be between 1.4 and 1.8.

We will focus our analysis on the dwarf star-forming galaxies with the highest quality spectra (i.e. those listed in Table 3), which limits our analysis to the most extreme EW $C\text{ III]}$ emitters. Two of the galaxies (863_348, MACS 0451-1.1) in Table 4 have detections of $C\text{ III]}$ and both components of the $O\text{ III] } \lambda\lambda 1661, 1666$ doublet. Another two galaxies (876_330, 860_359) have detections of $O\text{ III] } \lambda 1666$ and $C\text{ III] } \lambda 1908$ but no detection of $O\text{ III] } \lambda 1661$. Assuming an electron temperature of $T_e = 15\,000$ K (consistent with similarly metal-poor galaxies studied in Erb et al. 2010 and Christensen et al. 2012b), we find that $\log C^{+2}/O^{+2} = -1.0$ for 863_348 and $\log C^{+2}/O^{+2} = -0.8$ for MACS 0451-1.1. For 876_330 and 860_359, the observed line ratios indicate that $-1.1 < \log C^{+2}/O^{+2} < -0.8$ and $-0.8 < \log C^{+2}/O^{+2} < -0.6$, respectively. The presence of $C\text{ IV}$ emission in 863_348 and 860_359 indicates that a significant component of carbon is triply ionized and that the ICF will certainly be greater than unity. Allowing the ICF to be between 1.2 and 2.0, we find $-1.0 < \log C/O < -0.7$ for 863_348 and $-0.8 < \log C/O < -0.5$ for MACS 0451-1.1. Applying the same assumptions to 876_330 and 860_359, we find $-1.0 < \log C/O < -0.5$ and $-0.8 < \log C/O < -0.3$.

The C/O ratios of the metal-poor dwarf star-forming galaxies in our sample are much lower than the solar C/O ratio ($\log C/O = -0.26$) and the C/O ratio in Orion ($\log C/O = -0.21$; Esteban et al. 2004) but are similar to those of other metal-poor high-redshift galaxies (e.g. Erb et al. 2010; Christensen et al. 2012b; James et al. 2014), consistent with the framework described above in which the trend of C/O with O/H (for galaxies with $[O/H] > -1$) is set by metallicity-dependent winds in massive stars. Based on the ultraviolet spectra of our sample, it is clear that galaxies with low C/O ratios can still have very large EW $C\text{ III]}$ and $C\text{ IV}$ emission. While the reduced carbon abundance certainly impacts the observed $C\text{ III]}$ line strengths, the EWs remain very large owing to other factors (metal-poor gas, young and low-metallicity stars, large ionization parameter) which typically accompany galaxies with low C/O ratios.

5 PHOTOIONIZATION MODELLING

We now explore whether photoionization models can reproduce the ultraviolet emission-line ratios and EWs of the dwarf galaxies. First, we investigate whether the emission lines can be explained entirely by a low gas-phase metallicity, or if variations in the age, stellar metallicity, and ionization parameter are also required. Secondly, we examine whether there is enough energetic radiation output by

low-metallicity stellar populations to power the $C\text{ IV}$ emission seen in several dwarf systems.

5.1 Method

We appeal to new models by Gutkin et al. (in preparation) to compute the emission from the photoionized interstellar gas in star-forming galaxies. These models are based on the prescription of Charlot & Longhetti (2001), which combines a stellar population synthesis model with a photoionization code. In this approach, the ensemble of $H\text{ II}$ regions and the diffuse gas ionized by young stars throughout a galaxy are described by means of effective (i.e. galaxy-wide) parameters. The main adjustable parameters of the photoionized gas are the interstellar metallicity, Z , the typical ionization parameter of a newly ionized $H\text{ II}$ region, U (which characterizes the ratio of ionizing-photon to gas densities at the edge of the Strömgen sphere), and the dust-to-metal (mass) ratio, ξ_d (which characterizes the depletion of metals on to dust grains).

The solar relative ratios of C, N, and O adopted by Gutkin et al. to reproduce the optical emission-line ratios of a large sample of nearby SDSS galaxies are $(C/O)_\odot \approx 0.39$ and $(N/O)_\odot \approx 0.09$. By default, C/O is assumed to not vary with gas metallicity, while Gutkin et al. appeal to the relation of Groves, Dopita & Sutherland (2004, equation 5) to describe the dependence of N/O on metallicity. We also consider models with reduced C and N abundances at fixed metallicity, to describe the delayed release of C and N by intermediate-mass stars relative to shorter lived massive stars, which are the main production sites of O (and also produce C and N; Henry et al. 2000) in young galaxies. For simplicity, we follow Erb et al. (2010) and consider models in which C and N are reduced in equal proportions relative to the default values at fixed metallicity, by factors of between 0.85 and 0.05.

We also include attenuation of line and continuum photons by dust in the neutral ISM, using the two-component model of Charlot & Fall (2000), as implemented by da Cunha, Charlot & Elbaz (2008, their equations 1–4). This is parametrized in terms of the total V -band attenuation optical depth of the dust, $\hat{\tau}_V$, and the fraction μ of this arising from dust in the diffuse ISM rather than in giant molecular clouds. Accounting for these two dust components is important to describe the attenuation of emission-line EWs.

In their models, Gutkin et al. use the latest version of the Bruzual & Charlot (2003) stellar population synthesis code to compute the emission from stars. Following Charlot & Longhetti (2001), they neglect the contribution by stars older than 10 Myr to nebular emission and use the latest version of the standard photoionization code CLOUDY (Ferland et al. 2013) to compute the emission-line spectrum generated by younger stars, assuming that galaxies are ionization bounded. In all calculations, the stellar metallicity is taken to be the same as that of the interstellar gas. The models considered here assume constant SFR and a standard Chabrier (2003) IMF.

To interpret the nebular emission from the galaxies in our sample, we build a comprehensive grid of models covering a wide range of input parameters. Specifically, we take ionization parameters $\log U = -1.0, -1.5, -2.0, -2.5, -3.0, -3.5$, and -4.0 ; interstellar metallicities $Z = 0.0001, 0.0002, 0.0005, 0.001, 0.002, 0.004, 0.008, 0.017$, and 0.03 ; dust-to-metal ratios $\xi_d = 0.1, 0.3$, and 0.5 ; C/O (and N/O) scaling factors $1.0, 0.85, 0.65, 0.45, 0.25, 0.15$, and 0.05 ; about 70 model ages between 10 Myr and 1 Gyr; 10 attenuation optical depths $\hat{\tau}_V$ between 0 and 1; and, for each $\hat{\tau}_V$, 10 values of μ between 0 and 1. We adopt a Bayesian approach similar to that of Brinchmann et al. (2004, their equation 1) to compute the likelihood

Table 7. Properties of best-fitting (i.e. median) models and the 68 per cent confidence intervals for the low-mass galaxies in our sample with the best UV spectra (see Section 5.1 for details on modelling procedure). In the bottom three rows, we present a subset of the line flux ratios and equivalent widths of the median model.

Property	876_330	863_348	860_359	MACS 0451-1.1
$\log U$	$-2.16^{+0.27}_{-0.32}$	$-1.84^{+0.15}_{-0.21}$	$-2.13^{+0.16}_{-0.16}$	$-1.97^{+0.28}_{-0.30}$
$12 + \log(\text{O}/\text{H})$	$7.74^{+0.27}_{-0.56}$	$7.82^{+0.10}_{-0.53}$	$7.79^{+0.19}_{-0.46}$	$7.29^{+0.58}_{-0.22}$
$\log(\text{C}/\text{O})$	$-0.68^{+0.14}_{-0.17}$	$-0.74^{+0.08}_{-0.08}$	$-0.58^{+0.07}_{-0.08}$	$-0.71^{+0.13}_{-0.09}$
$\log(\text{age}/\text{yr})$	$7.55^{+0.79}_{-0.48}$	$6.75^{+0.52}_{-0.52}$	$7.30^{+0.56}_{-0.34}$	$7.71^{+0.74}_{-0.57}$
$\log\{W([\text{O III}]\lambda 4959, 5007 + \text{H}\beta)\}$	$2.84^{+0.25}_{-0.28}$	$3.18^{+0.09}_{-0.18}$	$3.00^{+0.18}_{-0.19}$	$2.78^{+0.24}_{-0.23}$
μ	$0.70^{+0.18}_{-0.39}$	$0.78^{+0.12}_{-0.35}$	$0.77^{+0.13}_{-0.38}$	$0.70^{+0.18}_{-0.39}$
$\hat{\tau}_V$	$0.20^{+0.40}_{-0.20}$	$0.01^{+0.22}_{-0.18}$	$0.14^{+0.42}_{-0.19}$	$0.19^{+0.38}_{-0.18}$
He II/C III]	0.006	0.005	0.004	0.002
C IV/C III]	0.438	0.892	0.404	1.113
EW(C III]	9.597	10.556	12.302	6.715

of each model given the data. The reader is directed to this work for more details.

5.2 Results

We focus our modelling efforts on the four dwarf star-forming galaxies with the highest quality spectra (876_330, 863_348, 860_359, MACS 0451-1.1). The C III] EWs spanned by this subset range from fairly typical values for dwarf star-forming systems (6.7 Å in MACS 0451-1.1) to the most extreme values in our sample (13.5 Å in 863_348). As our goal is to determine what is required to produce the ultraviolet spectra, we do not fit the continuum SEDs or optical spectral features. We instead find the range of models within our grid which provides the closest match to the EW of C III] and the flux ratios of C IV, O III] λ 1661, O III] λ 1666, Si III] λ 1883, and Si III] λ 1892 with respect to C III]. We do not include the He II/C III] ratio in the fitting process, as He II includes a stellar wind component which is non-trivial to decompose from the nebular component at low S/N (see Erb et al. 2010).

The properties of the best-fitting (i.e. median) models are listed in Table 7, revealing a very similar picture to that implied by the rest-

optical spectra and broad-band SEDs. The extreme UV emission-line strengths of our low-mass galaxies strongly favour models with low oxygen abundances (0.04–0.13 Z_{\odot}), young ages (6–50 Myr) for an assumed constant star formation history, large ionization parameters ($\log U = -2.16$ to -1.84), and low C/O ratios ($\log \text{C}/\text{O} = -0.74$ to -0.58). The probability density functions of $\log U$ and $12 + \log(\text{O}/\text{H})$ are shown in Fig. 8. We note that as with the modelling of the continuum SED, the ages are only valid for the assumed star formation history. More complicated star formation histories (i.e. those with a young and old component) would likely fit the data equally well as long as the recent star formation dominates the observed emission. Given the ease in fitting the emission lines with a single-component constant star formation history, we do not explore two-component models. As can be seen in Table 7, the models which best fit the ultraviolet spectra have large EW [O III]+H β emission lines (600–1500 Å rest frame). Not only are these values consistent with the observations in Section 4.3, but they provide further evidence for a close connection between the optical EELG population and the strong UV line emitters in our sample.

The first question we posed at the outset of this section was whether the prominent UV emission lines could be explained

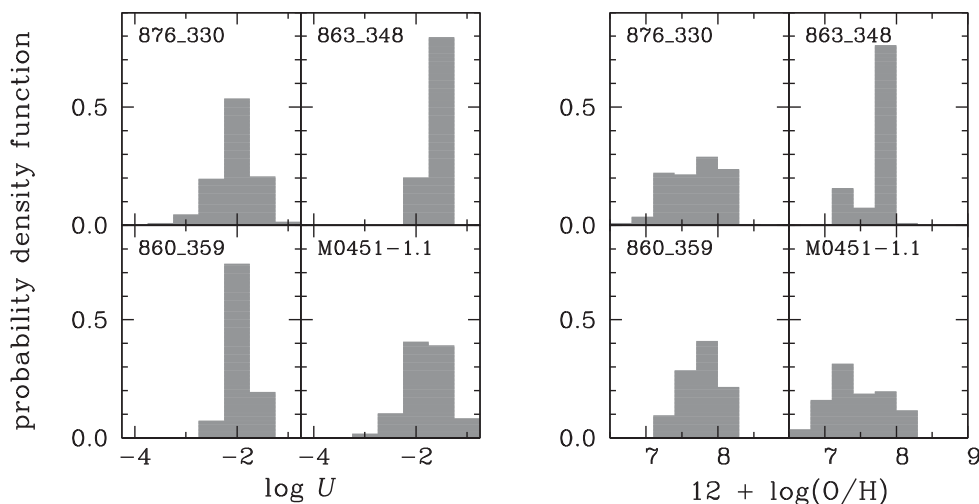


Figure 8. Results from photoionization modelling of C III] emitters (Section 5). To reproduce the extreme ultraviolet EWs, we require large ionization parameters (left-hand panel) and low-metallicity gas and massive stars (right-hand panel). The models also require young ages (best fits of 6–51 Myr) and subsolar carbon to oxygen abundances. Details of the best fits are provided in Table 7.

simply by the larger electron temperature that follows inefficient cooling in low-metallicity gas. The best-fitting parameters indicate that this is not the case. Stellar population ages must be considerably lower and ionization parameters somewhat larger than are commonly inferred for more massive star-forming systems at high redshift (e.g. Hainline et al. 2009; Richard et al. 2011a, Reddy et al. 2012b).

The second question we motivated was whether the large EW C IV emission seen in our most extreme galaxies could be powered by normal stellar populations without resorting to other energetic sources. The C IV/C III] ratios of the best-fitting models (Table 7) indicate that moderately low metallicity models with large ionization parameters produce ample energetic radiation to drive the observed C IV emission. We note that these same models predict weak He II λ 1640 emission, in agreement with the observations presented in Section 3.3. While further data are certainly required to determine if AGN, high-mass X-ray binaries, or fast radiative shocks help power the high-ionization emission lines, the models suggest that they are not required to explain the C IV emission.

6 DISCUSSION

6.1 New method of UV spectroscopy in reionization era

In this paper, we have demonstrated that several ultraviolet emission lines (C III], O III], C IV) have particularly large EWs in low-mass star-forming galaxies at high redshift. As a result of the attenuation of Ly α in $z \simeq 7$ galaxies (e.g. Ono et al. 2012; Pentericci et al. 2012; Schenker et al. 2012, Schenker et al. 2014; Treu et al. 2013), these UV emission lines likely provide our best hope of confirming very high redshift galaxies with ground-based facilities. Even if new infrared spectrographs soon begin to yield more detections of Ly α at $z \gtrsim 7$, it will remain difficult to draw conclusions on the nature of early galaxies owing to resonant scattering of Ly α by neutral hydrogen in the IGM. The ultraviolet emission lines described above provide an attractive alternative, opening the door for insight into the stellar populations and ionized gas conditions at $z \gtrsim 7$ through photoionization modelling of line ratios and EWs.

Based on our understanding of the physical conditions and stellar populations that produce large EW ultraviolet emission lines (as detailed in Section 5.2), we predict that C III] should be prominent in the spectra of $z \gtrsim 6$ galaxies. The blue UV slopes of $z \gtrsim 6$ galaxies (e.g. Bouwens et al. 2013; Dunlop et al. 2013) are very similar to our sample of C III] emitters at $z \simeq 2$ –3 and likely reflect low metallicities and minimal reddening. Once nebular emission contamination is accounted for at $z \gtrsim 6$, the sSFRs are found to be very large (Stark et al. 2013a; Gonzalez et al. 2014; de Barros, Schaerer & Stark 2014; Smit et al. 2014), pointing to an ionizing spectrum dominated by very massive stars. And perhaps the most important smoking gun comes from recent inferences of large EW rest-optical emission lines (Labbé et al. 2013; Stark et al. 2013a; Smit et al. 2014). Based on the photoionization models considered in Section 5.2, extreme rest-frame optical emission lines are almost always accompanied by large EW C III] emission in the rest-frame ultraviolet.

Detection of C III] in the reionization era need not wait for future facilities. For a bright ($H_{160} = 24.5$) gravitationally lensed galaxy at $z \simeq 6$, similar to many discovered recently (e.g. Richard et al. 2011b, Zitrin et al. 2012; Bradley et al. 2013), a C III] emitter with rest-frame EW between 7 and 13 Å would have a line flux (3 – 6×10^{-18} erg cm $^{-2}$ s $^{-1}$) which is readily detectable with existing spectrographs. In the brightest known $z \gtrsim 6$ galaxies ($J_{125} = 24.0$ in Zitrin et al.

2012), an extreme C III] emitter (similar to 863_348) could have line fluxes as bright as 1.4×10^{-17} erg cm $^{-2}$ s $^{-1}$, requiring no more than an hour for detection.

Because the C III] doublet is likely to be resolved by most ground-based spectrographs at $z \gtrsim 6$, the total flux quoted above will be split among two components. Integration times should be chosen to detect individual components. Care must also be taken to avoid sources that place C III] at wavelengths affected by sky lines and atmospheric absorption. Redshift between 5.2 and 6.1 will have C III] in the *J* band, and between $z = 6.9$ and 8.3 the line will be in the *H* band. To demonstrate the feasibility of detecting C III] at $z \gtrsim 6$, it makes sense to first focus on the small subset of bright sources with spectroscopic confirmation from Ly α . Not only does the presence of large EW Ly α increase confidence that C III] will be present (based on Fig. 4b), but for these sources, one can ensure that the observed wavelengths of C III], O III], and C IV are located in clean regions of the near-IR sky (after accounting for the small velocity offset between Ly α and systemic as discussed in Section 3.4).

Spectroscopic detection or robust limits on the EWs of C III], O III], and C IV would provide new insight into the nature of $z \gtrsim 6$ galaxies. If UV lines are detected, photoionization modelling of the line strengths (together with the broad-band SED) will yield much improved constraints on the age and metallicity of the stellar populations, allowing us to put better constraints on the ionizing output of galaxies in the reionization era (e.g. Robertson et al. 2013). In galaxies where Ly α is also present, detection of C III] will provide a measure of the systemic redshift, allowing Ly α to be shifted into the rest frame. The derived Ly α velocity profile would provide new constraints on the transfer of Ly α through the outflowing neutral gas surrounding the galaxy. By improving our understanding of how Ly α escapes from low-mass galaxies at $z \gtrsim 6$, we will be better equipped to map Ly α evolution at $z \gtrsim 6$ to the ionization state of the IGM.

6.2 Star formation in high-redshift low-mass galaxies

If stellar feedback is strong in low-mass galaxies, star formation histories are likely to be strongly variable or bursty. The imprint of such star formation fluctuations should be visible in the emission line and continuum properties of the lowest mass galaxies in our sample. In particular, the burstiness should cause the scatter in sSFRs to be greater in lower stellar mass galaxies. A natural consequence of this is that there should be a significant population of low-mass galaxies undergoing very rapid stellar mass growth. Such galaxies will be marked by large sSFRs and very large EW nebular emission lines. The data we have collected suggest that extreme line emitters with large ($\gtrsim 20$ Gyr $^{-1}$) sSFRs are fairly common among low-luminosity star-forming galaxies, similar to other recent results (e.g. Atek et al. 2011; van der Wel et al. 2011). The most extreme systems in our sample, such as 863_348, require a hard radiation field from fairly young stellar populations ($\lesssim 10$ Myr), as might be expected for galaxies in the midst of a substantial upturn in their star formation.

If star formation does fluctuate rapidly in low-mass galaxies, then there should also be a population with very low sSFRs. If the period of low star formation activity lasts for $\gtrsim 10^7$ yr, such systems will lack the O and early B stars which power nebular emission lines. In contrast, as long as there has been significant star formation activity in the past 100 Myr, the UV continuum (which is powered by O through later B-type stars) will remain prominent. Both recombination and collisionally excited lines will thus be much weaker with respect to the UV continuum in this population. Because our

selection relies primarily on emission lines for redshift confirmation, our current sample is biased against finding low-mass galaxies with low sSFRs. But as we discussed in Sections 4.2 and 4.4, we do identify one low stellar mass ($5.1 \times 10^6 M_{\odot}$) system, 869_328, which might have recently undergone a downturn in its star formation. While the sSFR derived from the UV continuum reflects very rapid stellar mass growth over the past 100 Myr, all indications suggest that nebular emission (line and continuum) are much weaker than for other systems with similar stellar continuum properties. Either the region of the galaxy sampled by the slit has a large escape fraction of ionizing radiation, or the massive stars necessary to power nebular emission are absent owing to bursty star formation or a stochastic sampling of the IMF.

Of course having observed only 17 low-luminosity galaxies, a key question is whether the extreme UV and optical spectral features found in our sample are as common as implied by our data. As discussed above, our spectroscopic selection certainly biases us towards objects with emission lines (although it should be noted that the spectra are of sufficient quality to detect absorption lines and low-EW line emission), and at the lowest stellar masses we are somewhat biased towards objects with large sSFR because of our selection in the rest-frame UV. In the coming years, WFC3/IR observations of faint lensed galaxies in the *HST* Frontier Fields (GO: 13496, PI: Lotz, as well as through the WFC3/IR grism survey GLASS, GO 13459; PI: Treu) should enable a more uniform census of the rest-frame optical nebular emission line properties of very low mass galaxies at high redshift, allowing a more reliable determination of whether there is substantially more scatter in the sSFRs at low masses.

7 SUMMARY AND FUTURE OUTLOOK

We have presented observations of 17 low-luminosity ($M_{UV} = -13.7$ to -19.9) gravitationally lensed galaxies at $z \simeq 1.5$ – 3.0 . Stellar masses inferred from SED fitting range between 2.0×10^6 and $1.4 \times 10^9 M_{\odot}$ with a median of $6.3 \times 10^7 M_{\odot}$. Deep optical spectra reveal prominent ultraviolet emission lines rarely seen in more luminous galaxies. The blended C III] λ 1908 doublet is seen in 16 of 17 galaxies with an average EW of 7.1 \AA , four times greater than that seen in the composite spectrum of luminous LBGs at $z \simeq 3$ (Shapley et al. 2003). Many of the galaxies also show fainter emission from O III] λ 1661,1666 and Si III] λ 1883,1892. The most extreme C III] emitters in our sample have rest-frame EWs as large as 13.5 \AA . These systems also show prominent emission from C IV λ 1549, requiring a substantial flux of photons with energies greater than 47.9 eV, similar to the local population of blue compact dwarfs (e.g. Thuan & Izotov 2005). Notably, the nebular He II λ 1640 emission line is weak or non-detected in many of the C III] emitters. We demonstrate that the EW of C III] is correlated with that of Ly α at $z \simeq 2$ – 3 . Galaxies with Ly α EWs of greater than 50 \AA generally show C III] emission with EWs greater than 5 \AA .

With the goal of understanding the origin of the UV emission lines in our low-mass galaxies, we have explored the physical properties in more detail in Section 4. While the SFRs of our sample tend to be very low (median of $1.7 M_{\odot} \text{ yr}^{-1}$), the sSFRs are very large (median of 27 Gyr^{-1}), indicating that the galaxies are undergoing a period of rapid stellar mass growth. The continuum UV slopes are very blue (median of $\beta = -2.2$), likely reflecting minimal dust content, young ages, and low metallicity. The presence of powerful [O III]+H β emission is apparent from the broad-band SEDs, implying an average rest-frame EW (770 \AA) similar to the population of

EELGs identified in recent surveys. Near-infrared spectra obtained with Magellan/FIRE confirm the presence of strong rest-optical emission lines in a subset of our sample. Oxygen abundances derived for extreme C III] emitters indicate moderately metal poor gas ($\lesssim 0.2 Z_{\odot}$), while the only object without C III] emission appears to be somewhat more metal rich (0.4 – $0.5 Z_{\odot}$).

In Section 5, we have considered whether the UV emission lines can be reproduced by a new suite of photoionization models developed in Gutkin et al. (in preparation). We find that the extreme C III]-emitting galaxies in our sample require models with large ionization parameters ($\log U = -2.16$ to -1.84), metal-poor gas (0.04 – $0.13 Z_{\odot}$), subsolar C/O ratios ($\log C/O = -0.74$ to -0.58), and a hard radiation field from moderately metal poor and young (6 – 50 Myr for constant star formation history) massive stars. While the models suggest that AGN are not required to power the C IV emission lines, further observations are required to determine if additional heating sources are present.

The data and models support a physical picture whereby the prominent UV emission lines arise from a confluence of factors. The hard radiation field from young low-metallicity stars increases the electron temperature in the ionized gas, which in turn increases the strength of collisionally excited emission lines. The large sSFRs indicates an enhanced ionizing photon output per unit mass, increasing the EW of nebular emission lines. We suggest that the ubiquity of very large sSFRs in the low-luminosity galaxies in our sample may reflect a recent upturn (or burst) in star formation. Future work with more uniformly selected samples are required to further investigate the star formation histories implied by the ubiquity of large EW emission lines in low-mass galaxies at high redshift.

Given the strong attenuation of Ly α in $z \gtrsim 6.5$ galaxies (e.g. Ono et al. 2012; Pentericci et al. 2012; Schenker et al. 2012, 2014; Treu et al. 2013), we have argued that C III] is likely to be the strongest UV spectral feature in $z \gtrsim 7$ galaxies. Since ground-based studies are limited to the rest-UV at $z \gtrsim 6$, C III] may provide our best window on early galaxy formation in the era of 20–30 m class telescopes. While the infrared spectroscopic capability of *James Webb Space Telescope* will enable rest-optical lines to be detected to $z \simeq 8$ – 10 , at yet higher redshifts, C III], O III], and C IV are likely our best hope for redshift confirmation and detailed study. But detection of C III] does not have to wait for future facilities. We demonstrate that C III] should be detectable in bright ($H \lesssim 25$) gravitationally lensed galaxies now being located in *HST* imaging surveys (e.g. Richard et al. 2011b, Zitrin et al. 2012; Bradley et al. 2013). In the brightest of these, multiple UV lines should be present, enabling new constraints on the stellar populations and ionized gas conditions in reionization-era galaxies.

ACKNOWLEDGEMENTS

We thank the anonymous referee for a valuable report which strengthened the paper. We also thank Richard Ellis, Dawn Erb, Max Pettini, and Alice Shapley for enlightening conversations. WRF is grateful to Brad Holden for help with reduction of the Keck/LRIS data. DPS acknowledges support from the National Science Foundation via grant AST-1410155. JR acknowledges support from the European Research Council (ERC) starting grant CALENDs and the Marie Curie Career Integration Grant 294074. SC, JG, and AW acknowledge support from the ERC via an Advanced Grant under grant agreement no. 321323NEOGAL. RA acknowledges support from the Swedish Research Council and the Swedish National Space Board. This paper includes data gathered with the 6.5 m Magellan Telescopes located at Las Campanas Observatory, Chile.

Some of the data presented herein were obtained at the W.M. Keck Observatory, which is operated as a scientific partnership among the California Institute of Technology, the University of California and the National Aeronautics and Space Administration. The Observatory was made possible by the generous financial support of the W.M. Keck Foundation. Based on observations made with ESO telescopes at the La Silla Paranal Observatory under programme 088.A-0571.

REFERENCES

- Akerman C. J., Carigi L., Nissen P. E., Pettini M., Asplund M., 2004, *A&A*, 414, 931
- Alavi A. et al., 2014, *ApJ*, 780, 143
- Alexandroff R. et al., 2013, *MNRAS*, 435, 3306
- Amanullah R. et al., 2011, *ApJ*, 742, L7
- Amorín R. et al., 2014, preprint ([arXiv:1403.3441](https://arxiv.org/abs/1403.3441))
- Anders P., Fritze-v. A. U., 2003, *A&A*, 401, 1063
- Asplund M., Grevesse N., Sauval A. J., Scott P., 2009, *ARA&A*, 47, 481
- Atek H. et al., 2011, *ApJ*, 743, 121
- Atek H. et al., 2014a, *ApJ*, 786, 60
- Atek H. et al., 2014b, *ApJ*, 789, 96
- Atek H. et al., 2014, preprint ([arXiv:1409.0512](https://arxiv.org/abs/1409.0512))
- Bayliss M. B., 2012, *ApJ*, 744, 156
- Bayliss M. B., Rigby J. R., Sharon K., Wuyts E., Florian M., Gladders M. D., Johnson T., Oguri M., 2014, *ApJ*, 790, 144
- Behroozi P. S., Wechsler R. H., Conroy C., 2013, *ApJ*, 770, 57
- Belokurov V., Evans N. W., Hewett P. C., Moiseev A., McMahon R. G., Sanchez S. F., King L. J., 2009, *MNRAS*, 392, 104
- Bensby T., Feltzing S., 2006, *MNRAS*, 367, 1181
- Bouwens R. J. et al., 2012, *ApJ*, 754, 83
- Bouwens R. J. et al., 2013, *ApJ*, preprint ([arXiv:1306.2950](https://arxiv.org/abs/1306.2950))
- Bradley L. D. et al., 2013, preprint ([arXiv:1308.1692](https://arxiv.org/abs/1308.1692))
- Brammer G. B. et al., 2012, *ApJ*, 758, L17
- Brinchmann J., Charlot S., White S. D. M., Tremonti C., Kauffmann G., Heckman T., Brinkmann J., 2004, *MNRAS*, 351, 1151
- Broadhurst T. et al., 2005, *ApJ*, 621, 53
- Bruzual G., Charlot S., 2003, *MNRAS*, 344, 1000
- Bunker A. J. et al., 2010, *MNRAS*, 409, 855
- Calzetti D., Armus L., Bohlin R. C., Kinney A. L., Koornneef J., Storchi-Bergmann T., 2000, *ApJ*, 533, 682
- Chabrier G., 2003, *PASP*, 115, 763
- Charlot S., Fall S. M., 2000, *ApJ*, 539, 718
- Charlot S., Longhetti M., 2001, *MNRAS*, 323, 887
- Christensen L. et al., 2012a, *MNRAS*, 427, 1953
- Christensen L. et al., 2012b, *MNRAS*, 427, 1973
- Coe D., Bradley L., Zitrin A., 2014, preprint ([arXiv:1405.0011](https://arxiv.org/abs/1405.0011))
- Conroy C., Wechsler R. H., 2009, *ApJ*, 696, 620
- Cooke R., Pettini M., Steidel C. C., Rudie G. C., Nissen P. E., 2011, *MNRAS*, 417, 1534
- da Cunha E., Charlot S., Elbaz D., 2008, *MNRAS*, 388, 1595
- de Barros S., Schaerer D., Stark D. P., 2014, *A&A*, 563, A81
- Dekel A., Silk J., 1986, *ApJ*, 303, 39
- Diehl H. T. et al., 2009, *ApJ*, 707, 686
- Dunlop J. S. et al., 2013, *MNRAS*, 432, 3520
- Efstathiou G., 1992, *MNRAS*, 256, 43
- Erb D. K., Pettini M., Shapley A. E., Steidel C. C., Law D. R., Reddy N. A., 2010, *ApJ*, 719, 1168
- Esteban C., Peimbert M., García-Rojas J., Ruiz M. T., Peimbert A., Rodríguez M., 2004, *MNRAS*, 355, 229
- Fabbian D., Nissen P. E., Asplund M., Pettini M., Akerman C., 2009, *A&A*, 500, 1143
- Ferland G. J., Korista K. T., Verner D. A., Ferguson J. W., Kingdon J. B., Verner E. M., 1998, *PASP*, 110, 761
- Ferland G. J. et al., 2013, *Rev. Mex. Astron. Astrofis.*, 49, 137
- Finkelstein S. L. et al., 2012, *ApJ*, 756, 164
- Förster Schreiber N. M. et al., 2009, *ApJ*, 706, 1364
- Fosbury R. A. E. et al., 2003, *ApJ*, 596, 797
- Frye B. L. et al., 2007, *ApJ*, 665, 921
- Garnett D. R., Skillman E. D., Dufour R. J., Peimbert M., Torres-Peimbert S., Terlevich R., Terlevich E., Shields G. A., 1995, *ApJ*, 443, 64
- Garnett D. R., Skillman E. D., Dufour R. J., Shields G. A., 1997, *ApJ*, 481, 174
- Garnett D. R., Shields G. A., Peimbert M., Torres-Peimbert S., Skillman E. D., Dufour R. J., Terlevich E., Terlevich R. J., 1999, *ApJ*, 513, 168
- Gonzalez V., Bouwens R., Illingworth G., Labbé I., Oesch P., Franx M., Magee D., 2014, *ApJ*, 781, 34
- Groves B. A., Dopita M. A., Sutherland R. S., 2004, *ApJS*, 153, 9
- Guo Q., White S., Li C., Boylan-Kolchin M., 2010, *MNRAS*, 404, 1111
- Guseva N. G., Izotov Y. I., Thuan T. X., 2000, *ApJ*, 531, 776
- Hainline K. N., Shapley A. E., Kornei K. A., Pettini M., Buckley-Geer E., Allam S. S., Tucker D. L., 2009, *ApJ*, 701, 52
- Hainline K. N., Shapley A. E., Greene J. E., Steidel C. C., 2011, *ApJ*, 733, 31
- Hashimoto T., Ouchi M., Shimasaku K., Ono Y., Nakajima K., Rauch M., Lee J., Okamura S., 2013, *ApJ*, 765, 70
- Henry R. B. C., Edmunds M. G., Koumlyppen J., 2000, *ApJ*, 541, 660
- Holden B. P. et al., 2014, preprint ([arXiv:1401.5490](https://arxiv.org/abs/1401.5490))
- Hopkins P. F., Kereš D., Oñorbe J., Faucher-Giguère C.-A., Quataert E., Murray N., Bullock J. S., 2014, *MNRAS*, 445, 581
- Horne K., 1986, *PASP*, 98, 609
- James B. L. et al., 2014, *MNRAS*, 440, 1794
- Jones T. A., Swinbank A. M., Ellis R. S., Richard J., Stark D. P., 2010, *MNRAS*, 404, 1247
- Jones T., Ellis R. S., Richard J., Jullo E., 2013, *ApJ*, 765, 48
- Jullo E., Kneib J.-P., Limousin M., Elíasdóttir Á., Verdugo T., 2007, *New J. Phys.*, 9, 447
- Kelson D. D., 2003, *PASP*, 115, 688
- Kewley L. J., Dopita M. A., 2002, *ApJS*, 142, 35
- Kewley L. J., Ellison S. L., 2008, *ApJ*, 681, 1183
- Kneib J.-P., 1993, PhD thesis
- Kobulnicky H. A., Kewley L. J., 2004, *ApJ*, 617, 240 (KK04)
- Kobulnicky H. A., Skillman E. D., 1998, *ApJ*, 497, 601
- Koekemoer A. M. et al., 2007, *ApJS*, 172, 196
- Labbé I. et al., 2013, *ApJ*, 777, L19
- Larson R. B., 1974, *MNRAS*, 169, 229
- Lee J. C. et al., 2009, *ApJ*, 706, 599
- Limousin M. et al., 2007, *ApJ*, 668, 643
- McLure R. J. et al., 2013, *MNRAS*, 432, 2696
- Maseda M. V. et al., 2013, *ApJ*, 778, L22
- Masters D. et al., 2014, *ApJ*, 785, 153
- Moster B. P., Somerville R. S., Maulbetsch C., van den Bosch F. C., Macciò A. V., Naab T., Oser L., 2010, *ApJ*, 710, 903
- Murray N., Quataert E., Thompson T. A., 2005, *ApJ*, 618, 569
- Oesch P. A. et al., 2010, *ApJ*, 725, L150
- Oesch P. A. et al., 2012, *ApJ*, 759, 135
- Oke J. B., Gunn J. E., 1983, *ApJ*, 266, 713
- Oke J. B. et al., 1995, *PASP*, 107, 375
- Ono Y. et al., 2012, *ApJ*, 744, 83
- Osterbrock D. E., 1989, Research supported by the University of California, John Simon Guggenheim Memorial Foundation, University of Minnesota, et al. University Science Books, Mill Valley, CA
- Osterbrock D. E., Ferland G. J., 2006, *Astrophysics of Gaseous Nebulae and Active Galactic Nuclei*. Astrophysics of Gaseous Nebulae and Active Galactic Nuclei, 2nd edn. University Science Books, Mill Valley, CA
- Pacifici C., Charlot S., Blaizot J., Brinchmann J., 2012, *MNRAS*, 421, 2002
- Papovich C., Dickinson M., Ferguson H. C., 2001, *ApJ*, 559, 620
- Pentericci L., 2011, *ApJ*, 743, 132
- Pettini M., Pagel B. E. J., 2004, *MNRAS*, 348, L59 (PP04)
- Pettini M., Rix S. A., Steidel C. C., Adelberger K. L., Hunt M. P., Shapley A. E., 2002, *ApJ*, 569, 742
- Pontzen A., Governato F., 2012, *MNRAS*, 421, 3464

- Price S. H. et al., 2014, *ApJ*, 788, 86
- Quider A. M., Pettini M., Shapley A. E., Steidel C. C., 2009, *MNRAS*, 398, 1263
- Quider A. M., Shapley A. E., Pettini M., Steidel C. C., Stark D. P., 2010, *MNRAS*, 402, 1467
- Reddy N. A., Steidel C. C., 2009, *ApJ*, 692, 778
- Reddy N. et al., 2012a, *ApJ*, 744, 154
- Reddy N. A., Pettini M., Steidel C. C., Shapley A. E., Erb D. K., Law D. R., 2012b, *ApJ*, 754, 25
- Richard J. et al., 2007, *ApJ*, 662, 781
- Richard J. et al., 2010, *MNRAS*, 404, 325
- Richard J., Jones T., Ellis R., Stark D. P., Livermore R., Swinbank M., 2011a, *MNRAS*, 413, 643
- Richard J., Kneib J.-P., Ebeling H., Stark D. P., Egami E., Fiedler A. K., 2011b, *MNRAS*, 414, L31
- Robertson B. E., Ellis R. S., Dunlop J. S., McLure R. J., Stark D. P., 2010, *Nature*, 468, 49
- Robertson B. E. et al., 2013, *ApJ*, 768, 71
- Rogers A. B., McLure R. J., Dunlop J. S., 2013, *MNRAS*, 429, 2456
- Salpeter E. E., 1955, *ApJ*, 121, 161
- Santos M. R., Ellis R. S., Kneib J.-P., Richard J., Kuijken K., 2004, *ApJ*, 606, 683
- Schenker M. A., Stark D. P., Ellis R. S., Robertson B. E., Dunlop J. S., McLure R. J., Kneib J.-P., Richard J., 2012, *ApJ*, 744, 179
- Schenker M. A. et al., 2013a, *ApJ*, 768, 196
- Schenker M. A., Ellis R. S., Konidaris N. P., Stark D. P., 2013b, *ApJ*, 777, 67
- Schenker M. A., Ellis R. S., Konidaris N. P., Stark D. P., 2014, *ApJ*, preprint ([arXiv:1404.4632](https://arxiv.org/abs/1404.4632))
- Schmidt K. B. et al., 2014, *ApJ*, 782, L36
- Shapley A. E., 2011, *ARA&A*, 49, 525
- Shapley A. E., Steidel C. C., Pettini M., Adelberger K. L., 2003, *ApJ*, 588, 65
- Shapley A. E., Steidel C. C., Erb D. K., Reddy N. A., Adelberger K. L., Pettini M., Barmby P., Huang J., 2005, *ApJ*, 626, 698
- Shen S., Madau P., Conroy C., Governato F., Mayer L., 2013, *ApJ*, preprint ([arXiv:1308.4131](https://arxiv.org/abs/1308.4131))
- Shim H., Chary R.-R., Dickinson M., Lin L., Spinrad H., Stern D., Yan C.-H., 2011, *ApJ*, 738, 69
- Shirazi M., Brinchmann J., 2012, *MNRAS*, 421, 1043
- Simcoe R. A. et al., 2013, *PASP*, 125, 270
- Smit R. et al., 2014, *ApJ*, 784, 58
- Smith G. P., Kneib J.-P., Smail I., Mazzotta P., Ebeling H., Czoske O., 2005, *MNRAS*, 359, 417
- Stark D. P., Ellis R. S., Bunker A., Bundy K., Targett T., Benson A., Lacy M., 2009, *ApJ*, 697, 1493
- Stark D. P., Ellis R. S., Chiu K., Ouchi M., Bunker A., 2010, *MNRAS*, 408, 1628
- Stark D. P., Ellis R. S., Ouchi M., 2011, *ApJ*, 728, L2
- Stark D. P. et al., 2013a, *MNRAS*, 436, 1040
- Stark D. P., Schenker M. A., Ellis R., Robertson B., McLure R., Dunlop J., 2013b, *ApJ*, 763, 129
- Steidel C. C., Erb D. K., Shapley A. E., Robertson B., McLure R., Dunlop J., 2010, *ApJ*, 717, 289
- Stinson G. S., Dalcanton J. J., Quinn T., Kaufmann T., Wadsley J., 2007, *ApJ*, 667, 170
- Tapken C., Appenzeller I., Noll S., Richling S., Heidt J., Meinkhn E., Mehlert D., 2007, *A&A*, 467, 63
- Teyssier R., Pontzen A., Dubois Y., Read J. I., 2013, *MNRAS*, 429, 3068
- Thuan T. X., Izotov Y. I., 2005, *ApJS*, 161, 240
- Treu T., Schmidt K. B., Trenti M., Bradley L. D., Stiavelli M., 2013, *ApJ*, 775, L29
- van der Wel A. et al., 2011, *ApJ*, 742, 111
- Vanzella E. et al., 2010, *A&A*, 513, A20
- Vernet J. et al., 2011, *A&A*, 536, A105
- Wild V., Charlot S., Brinchmann J., Heckman T., Vince O., Pacifici C., Chevallard J., 2011, *MNRAS*, 417, 1760
- Wilkins S. M., Bunker A. J., Stanway E., Lorenzoni S., Caruana J., 2011, *MNRAS*, 417, 717
- Wuyts S. et al., 2011, *ApJ*, 738, 106
- Yuan T.-T., Kewley L. J., Rich J., 2013, *ApJ*, 767, 106
- Zitrin A. et al., 2012, *ApJ*, 747, L9

This paper has been typeset from a $\text{\TeX}/\text{\LaTeX}$ file prepared by the author.